Dynamic FEM assessment of sagbend

Improved methodology for the dynamic FEM assessment

Gijs-Jan Otten

Technische Universiteit Delft

TU Delft

Dynamic FEM assessment of sagbend

Improved methodology for the dynamic FEM assessment

by

Gijs-Jan Otten

In partial fulfillment of the requirements of the degree of

Master of Science

in Offshore and Dredging Engineering at the Delft University of Technology,
to be defended publicly on Friday 22nd of December 2017 at 03:00 PM.

Student number:	4086155	
Project duration:	February 1, 2017 – December 31, 2017	
Thesis committee:	Prof. Dr. A. V. Metrikine,	TU Delft
	Ir. Y. Qu,	TU Delft
	Dr. Ir. H. Hendrikse,	TU Delft
	Ir. H. Smienk,	HMC
	Ir. F. Kortekaas,	HMC

TU Delft

MARINE CONTRACTORS

Abstract

Heerema Marine Contractors (HMC) is a world leading marine contractor in the oil and gas industry. HMC's operations consist, among others, of subsea pipelines and infrastructures in shallow, deep and ultra-deep waters. In order to fulfil their vision of becoming the best offshore construction contractor in the world in carefully selected segments and regions of the market, they need to improve and optimize their performance. That includes a good understanding of the dynamic behaviour of the pipeline during installation.

One of the aspects that needs to be investigated in more detail is the dynamic behaviour of the pipe in sagbend region during flowline or riser installation. During pipelay, the pipeline is installed on the seabed using a J/R-lay installation vessel. The pipeline consists of a straight upper part and a curved lower part. The latter is called the sagbend. In this region there are several loads acting on the pipe as well as the external water pressure when installing the pipeline in empty condition. This results in the dynamic assessment of the sagbend being an important and sometimes governing load case for wall thickness design.

The current approach of the Finite Element Method (FEM) assessment of the sagbend is obtaining the maximum bending moment from dynamic global analyses and applying this on a static local model of the sagbend. Next to interface issues with the different software packages, it is also a conservative approach. Therefore the demand rose to improve this dynamic FEM assessment of the sagbend. This results in the research question: *"How could Frequency Based Dynamic Substructuring improve and speed up the dynamic FEM assessment of a pipe section in the sagbend region, without affecting robustness and reliability?"*

An enhanced methodology with the use of dynamic substructuring is proposed. With the dynamic substructuring, parts of the structure are replaced by dynamic stiffness matrices (DSM). These DSMs contain the dynamic response behaviour of the parts they replace. The responses of both the local and global models should be identical, but the local model with the DSMs has significantly reduced model size.

First the enhanced methodology is used for an analytical equivalent model consisting of a vertical Bernoulli beam. From this analytical analysis the conclusion is drawn that the dynamic substructuring method gives correct responses for the local model and is a promising method for the FEM assessment.

Then the enhanced methodology is applied to the FEM model in the Flexcom software. The DSMs were applied at the boundaries of the sagbend with the use of subroutines. Although these results are promising, further research is required to replace the current methodology.

The final conclusion is that the dynamic substructuring is a quick and effective method for analysing dynamic models. Although the application of the method to FEM was not successful, the application to the analytical model proved that it is still a promising method and further research should be performed on the use of dynamic stiffness matrices in a subroutine.

Preface

Dear reader,

Thank you for taking the time to read this documentation of my graduation thesis. It has been a challenging research project due to the theoretical complexity, but highly rewarding due to the better understanding of the phenomena afterwards. The thesis has been written to fulfil the graduation requirements of the master's program Offshore and Dredging Engineering at the Delft University of Technology.

I would like to thank all members of my graduation committee, as without them this thesis would not have been possible. The daily guidance and thorough feedback from Ir. Henk Smienk and Ir. Ferry Kortekaas at Heerema proved invaluable and are very much appreciated. Furthermore the analytical view and critical questions of Ir. Yang Qu are greatly valued. Also the experience of Dr. Ir. Hayo Hendrikse aided me in exposing and understanding the challenges of the research. Finally I would like to thank Prof. Dr. Andrei Metrikine as the chairman of my committee for his endless enthusiasm, feedback and of course encouragements during my whole thesis.

Last but definitely not least I would also like to thank my family, friends and girlfriend for their support and encouragements during this graduation project. This includes my fellow graduation students in sharing experiences, drinking bakkies and making doing this thesis so much more than solitary research.

Gijs-Jan Otten
Leiden, 29 December 2017

Acronyms

CMS	Component Mode Synthesis
Dd	drag diameter
DNV	Det Norske Veritas
DOF	Degree of Freedom
DSM	Dynamic Stiffness Matrix
EoM	Equation of Motion
FBS	frequency based substructuring
FEM	Finite Element Method
FFT	Fast Fourier Transform
FRF	Frequency Response Function
GNL	geometric nonlinear
HMC	Heerema Marine Contractors
LRFD	Load and Resistance Factor Design
OD	outer diameter
PDE	partial differential equation
RAO	Response Amplitude Operator
SpeRA	Spectral Response Analysis
TDP	touchdown point

List of Symbols

Greek Symbols

α_c	Flow stress parameter	-
α_p	Factor to account for effect of D/t_2 ratio	-
γ_m	Material strength factor	-
γ_{SC}	Safety Class resistance factor	-
Ω	Frequency	rad/s
Ω_{ex}	Excitation frequency	rad/s
ϕ	Coefficient of viscosity	Pa · s
ρ	Density	kg/m^3
θ	Rotation	rad

Roman Symbols

Y	Compliant stiffness matrix	
Z	Dynamic stiffness matrix	
A	Cross section area of the beam	m^2
c_d	Distributed damping coefficient	kg/s
C_a	Added mass coefficient	-
C_D	Dimensionless drag coefficient	-
C_M	Dimensionless inertia coefficient	-
E	Young's modules	GPa
I	Second moment of area	m^4
L	Length	m
M_p	Plastic moment capacity	Nm
M_{Sd}	Design moment	Nm
p_c	Characteristic collapse pressure	Pa
p_e	External pressure	Pa
p_i	Internal pressure	Pa
p_{min}	Minimal internal pressure	Pa
S_p	Plastic effective axial force capacity	N
S_{Sd}	Design effective axial force	N
t_2	Wall thickness	m
$u(t)$	Fluid velocity	m/s
$v(t)$	Velocity of a moving body	m/s
$W(x)$	Displacement	m

Sign convention

Due to the extensive use of Flexcom for this research the sign convention and axis system of this software is governing, see figure 1. Unless specifically stated differently the axis system of the Flexcom software shown in figure 1b is used in this thesis.

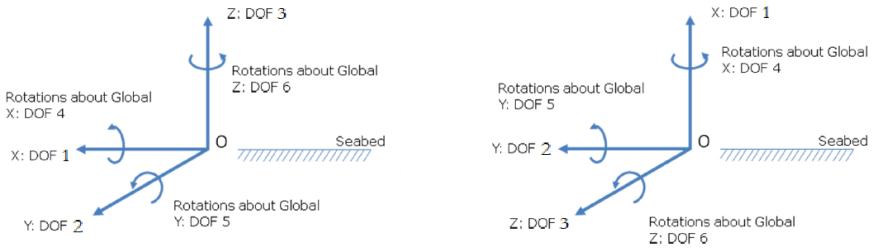

(a) Conventional axis system (b) Axis system Flexcom

Figure 1: Different axis systems used

Furthermore the sign convention of the forces and displacements is shown in 2. With the force convention on the left and the displacement on the right.

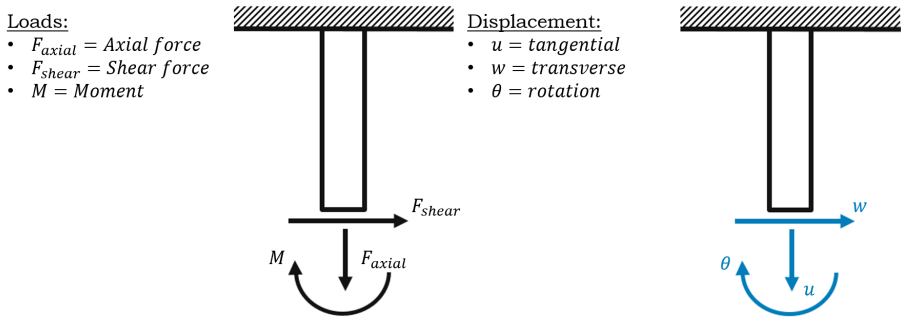

Figure 2: Sign convention of loads and displacements

Contents

1 Introduction

Heerema Marine Contractors (HMC) is a world leading marine contractor in the oil and gas industry. HMC specialises in the transport, installation and removal of offshore facilities. Among others these consist of fixed and floating structures, subsea pipelines and infrastructures in shallow, deep and ultra deep waters. HMC optimises its operations with a good understanding of all aspects involved. One of these aspects is the dynamic behaviour of the pipeline during installation. This dynamic behaviour is caused by vessel motions, waves and current. For this thesis the main focus is on the dynamic behaviour of the pipe in sagbend region during flowline or riser installation. In this chapter the challenges and the approach to take on these challenges are discussed.

1.1. Problem definition

During pipelay the pipeline is installed on the seabed using an installation vessel. The pipeline forms a catenary from the support on the vessel (hang-off table) to the touchdown point (TDP) on the seabed. The catenary consists of a straight part and a curved part. The latter part is called the sagbend region. In the sagbend region the pipeline orientation changes from a near vertical to the orientation of the seabed slope. At this region there are several loads acting on the pipe as well as a large pressure difference due to the external water pressure when installing the pipeline in empty condition. This results in the dynamic assessment of the sagbend being an important and sometimes governing load case for wall thickness design. This is especially the case if a different component, such as a counterbore, is present in the sagbend, see figure 1.1. A counterbore is a local reduction of the wall thickness at the pipe end and is applied to improve the fatigue performance of the girth weld.

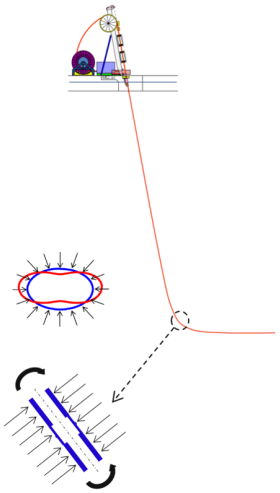

Figure 1.1: Schematic of pipelay with counterbore

During the tender phase of a project the engineers at HMC perform numerous calculations on this aspect of the pipeline installation. These calculations are done with complex models in two different types of Finite Element Method (FEM) software programs; *Flexcom* and *Abaqus*. Where Flexcom is used for the global dynamic analysis and Abaqus is used to analyse the local model statically, with the maximum dynamic bending moment from Flexcom as input. Unfortunately this is a time consuming approach with results that are an overestimation of reality due to the application of maximum bending moments from a dynamic analysis onto a static model. Moreover it is a method that is prone to errors due to interface issues between Flexcom and Abaqus, the main issues are different definition of internal forces and moments and different sign conventions for Flexcom and Abaqus shown in figure 1b and 1a respectively on page xi.

1.2. Objectives

The above mentioned downsides of the current method used by HMC create the need for a different methodology for dynamic assessment of the sagbend. Therefore, the main objective of this research is to develop a new methodology to perform a detailed dynamic FEM assessment of the sagbend. Requirements of this methodology are:

- **Efficient**: As the industry becomes more challenging and competitive, quicker and more efficient solutions are desired to stay ahead of competition. The objective is to perform the required calculations within 1 day.
- **Robust**: As HMC operates in a wide range of locations around the globe with different challenges, this methodology should be able to perform properly for different scenarios, e.g. water depth, varying pipe properties, sea states, etc.
- **Reliable**: The output should be reliable to maintain the high quality and safety standard HMC has set over the past decades.

In order to reach this main objective a secondary objective is formulated. The secondary objective is to study the application of dynamic stiffness, also known as super element or dynamic substructuring, at the boundaries of the cut-off of the local model. The principle of dynamic stiffness is to combine all the information about the dynamic response, above or below a cut-off, and replacing it by the dynamic stiffness; hence dynamic substructuring. All the information is gathered in a matrix, a so called Dynamic Stiffness Matrix (DSM). The result is a "one-way zoom" from the global to the local model, as is shown in figure 1.2. So instead of multiple time consuming iterations between global and local model, the calculations can be performed using only the local model without losing the influence of the global model.

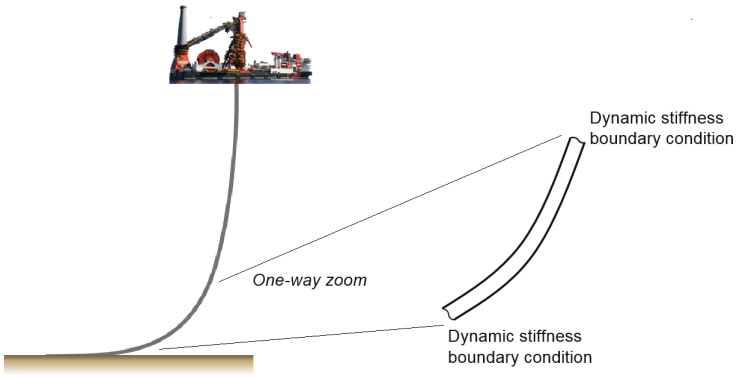

Figure 1.2: Schematic of one-way zoom approach

1.3. Research question

The above mentioned objectives lead the the formulation of the research question:

How could Frequency Based Dynamic Substructuring improve and speed up the dynamic FEM assessment of a pipe section in the sagbend region, without affecting robustness and reliability?

1.4. Approach of the research

The approach to reach the objectives is divided into 4 main steps. These are shown in figure 1.3 below. With the main steps in the blue squares and additional information in the white squares. Each step will be explained in short in the following paragraphs.

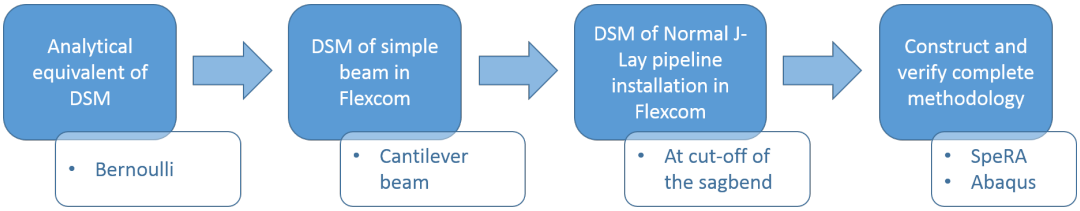

Figure 1.3: Flowchart of the methodology

Step 1: Analytical equivalent To get a better understanding of the principle of the DSM an analytical equivalent is studied. This analytical equivalent is a vertical Bernoulli beam, with distributed damping and hinges at the ends. From this analytical model a segment is cut out and the removed sections are replaced by DSMs.

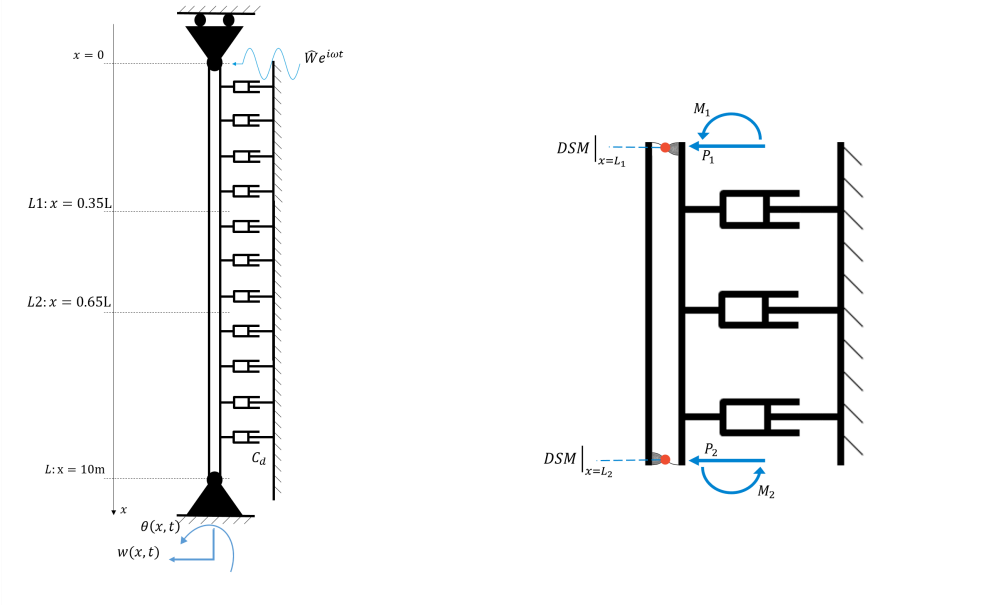

(a) Schematic of the analytical global model (b) Schematic of the local model, cut-out with DSMs

Figure 1.4: Analytical equivalent

Step 2: DSM of a simple beam The next step is to construct a simple model of a cantilever beam in the FEM software package Flexcom. One end is clamped and the other is free. The free end is then harmonically excited by an axial force, shear force and a moment independently. This results in a harmonic displacement and the ratio between the displacement and the force defines the Flexibility Matrix. Taking the inverse of this Flexibility matrix results in the DSM as is shown in equation 1.1. For a detailed explanation see section 4.2.1.

$$DSM = \left(FlexibilityMatrix\right)^{-1} = \left(\frac{ue^{i\omega t}}{Fe^{i\omega t}}\right)^{-1} = \left(\frac{u}{F}\right)^{-1} \tag{1.1}$$

This step is performed to check whether this approach to calculate a DSM with the use of a FEM software package, and for Heerema Flexcom software package in specific, is possible. It is more difficult to perform this check with the complex pipeline configuration, hence the simple beam.

Step 3: DSM of Normal J-Lay pipeline installation When the approach to calculate the DSM is verified in step 2, the same approach is applied on the pipeline. In this case the harmonic forces will be applied at the boundaries of the cut-out section. This results in a DSM for each cut-off as is shown in figure 1.5.

Step 4: Construction of methodology and verification The last step is to combine the calculated DSM with the HMC in house Spectral Response Analysis (SpeRA) tool to create the required input to perform a detailed dynamic FEM assessment of the cut-out section in the sagbend region using the FEM software Abaqus. The complete process of this methodology is shown below in figure 1.5.

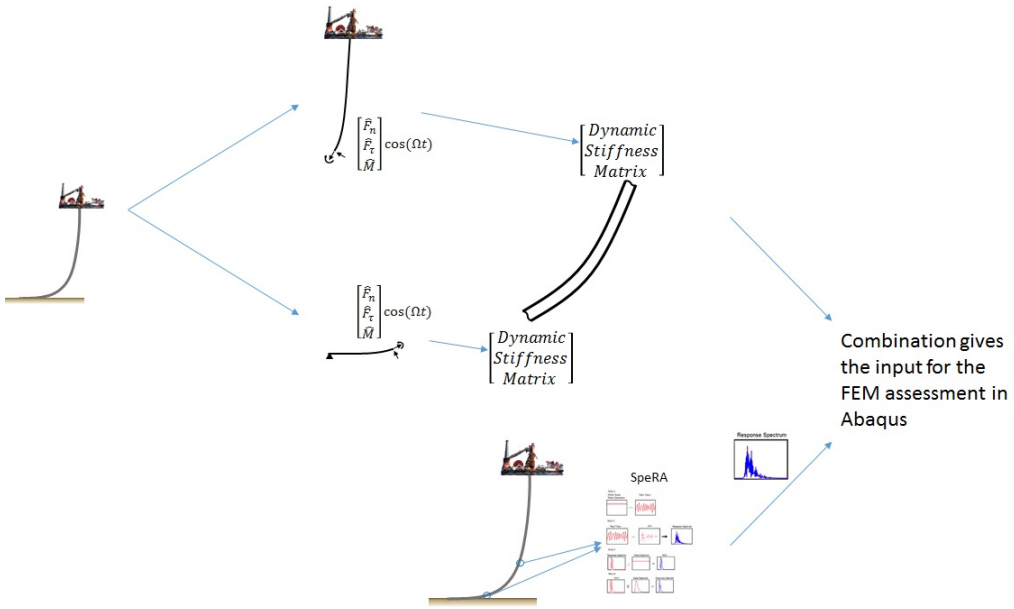

Figure 1.5: Schematic of the methodology

Verification of the methodology can be done by performing calculations for one and the same simple pipeline model, no component, and comparing the results of the DSM methodology with results from Flexcom. Note that Flexcom is accurate enough for basic dynamic response if no component is present, more difficult scenarios require the Abaqus software.

1.5. Report structure

First in chapter 2 the literature study is presented, which comprehends the topics with prerequisite knowledge and ends with the scope of this research. Chapter 3 describes the current method and the new enhanced methodology in more detail. After chapter 3 the structure of the report follows the 4 steps explained in section 1.4, with step 1 and 2 explained in 4. Followed by step 3 and 4 and the results of the new methodology in chapter 5. Finally the discussion in chapter 6 and the conclusions and recommendations are shown in chapter 7.

2

Literature study

This chapter discusses all the relevant topics that have been studied at the in order to gain the prerequisite knowledge for this research. Furthermore, this literature study was needed to be able to determine the scope of the research which is shown in section 2.6 of this chapter.

2.1. Installation methods

To understand and investigate the loads during pipeline installations, first the different methods of installation need to be studied. There are three common methods that are used to install pipelines on the seabed:

- S-lay
- J-lay
- Reel-lay, also known as R-lay

The S-lay method is not used by HMC, so this method will not be discussed in this thesis. The other two, J-lay and Reel-lay, are used by HMC. These two methods are similar, the main differences are the feed of pipeline to the tower and the effects of residual ovality and stresses caused by the Reel-lay method. Both methods experience the same axial tension and external pressure when lowered below the vessel. The effective tension depends on whether the pipe is installed empty or flooded. As mentioned in the introduction, the bending moment exists only in the sagbend and during the final stage. When the pipeline lays on the seabed, the external pressure is governing. Internal loads and strains in the pipeline can be controlled by changing the tower angle. The tower can be seen as the near vertical black structure in both figure 2.1a and 2.1b.

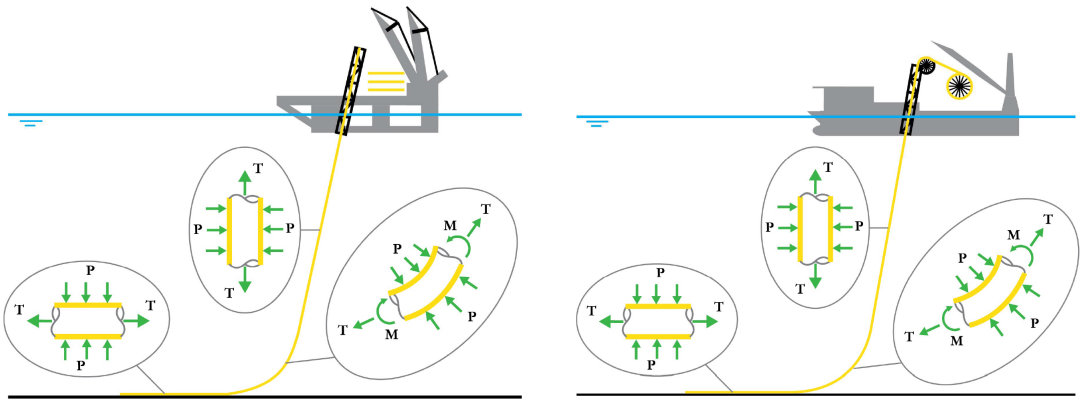

(a) Schematic representation of J-Lay

(b) Schematic representation of Reel-Lay

Figure 2.1: Installation methods used by HMC

J-lay

This installation method owes its name to the shape of the suspended pipeline, known as the catenary, which resembles the letter "J". This can be seen in figure 2.1a. For this installation method, prefabricated pipe segments are fed into the tower, where they are welded to the suspended pipeline. This method is suitable for deep water installations and large outer diameters (ODs).

Reel-lay

For a Reel-lay installation the pipeline segments are welded, coated and reeled onto a drum at an onshore location, a so-called spoolbase. This drum is either already located on board or transported and loaded on to the vessel. The next step is to reel the pipeline of the drum through straighteners into the tower and lower it towards the seabed. The reeling and unreeling of the pipeline causes plastic deformation that could negatively influence the load resistance of the pipeline.

For this research the focus was on the J-lay method. The residual ovalities and stresses caused by reeling would result in more complicated load case scenarios.

2.2. Sagbend

As mentioned in the introduction, the sagbend is the curved stretch of pipe where the pipeline changes from near vertical to horizontal orientation, indicated in figure 2.2.

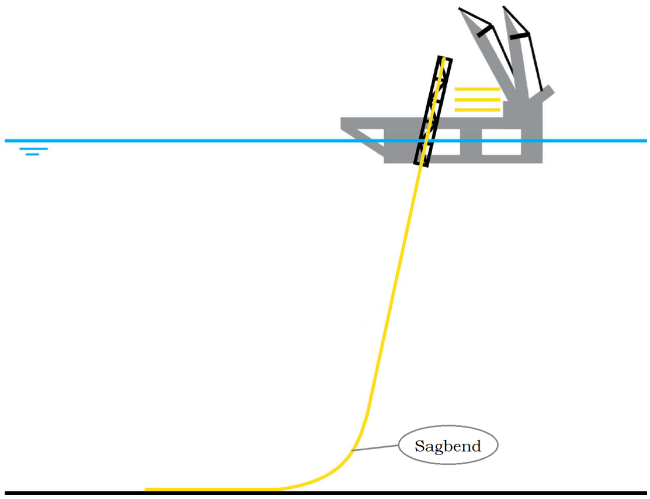

Figure 2.2: Sagbend for J-lay installation

The sagbend region will govern the wall thickness design for the pipeline in many cases. This is due to the active bending, low tension and external pressure on the pipeline. The sagbend is controlled by the submerged weight, the top tension, tower angle and to a lesser extent the flexural rigidity of the pipeline. In order to guarantee safety during installation procedures the international classification society Det Norske Veritas (DNV) investigated this behaviour and dedicated a section to it in their service document *Offshore Standard: Submarine Pipeline Systems* [3]. The general practice within the industry is to use the Load and Resistance Factor Design (LRFD) format. This design format is based on a limit state and partial safety factor methodology. The consequences of the failure define the load and resistance factors on the safety class. Section 5.607 of DNV-OS-F101 [3] applies for the sagbend region. This section gives the design criterion for pipe members subjected to bending moment, effective axial force and external overpressure.

$$\left\{\gamma_m \cdot \gamma_{SC} \cdot \frac{|M_{Sd}|}{\alpha_c \cdot M_p(t_2)} + \left\{\frac{\gamma_m \cdot \gamma_{SC} \cdot S_{Sd}}{\alpha_c \cdot S_p(t_2)}\right\}^2\right\}^2 + \left(\gamma_m \cdot \gamma_{SC} \cdot \frac{p_e - p_{min}}{p_c(t_2)}\right)^2 \leq 1 \tag{2.1}$$

$$15 \leq D/t_2 \leq 45\,, \qquad P_i < P_e\,, \qquad |S_{Sd}|/S_p < 0.4$$

Where:

- γ_m : Material strength factor [-]
- γ_{SC} : Safety Class resistance factor [-]
- M_p : Plastic moment capacity [Nm]
- M_{Sd} : Design moment [Nm]
- p_e : External pressure [Pa]
- p_i : Internal pressure [Pa]
- S_p : Plastic effective axial force capacity [N]
- S_{Sd} : Design effective axial force [N]
- t_2 : Wall thickness [m], Note: $t_2 = t_{nominal}$ for installation

And p_{min} and p_c are defined as:

p_{min} :The minimum internal pressure that can be sustained. This is normally taken as zero for installation except for cases where the pipeline is installed water filled.

p_c :The characteristic collapse pressure based on thickness t_2. The characteristic collapse pressure is defined as $p_e - p_{min} \leq \frac{p_c(t_2)}{\gamma_m \cdot \gamma_{SC}}$

In deeper water the normative buckling criteria should also be satisfied, due to potential collapse of the pipeline. Both buckling and collapse are defined by DNV. Where buckling is defined as:

> "A gross deformation of the cross section"

And where collapse is defined as:

> "The loss of load bearing capacity of the structure"

Finally it should be noted that the maximum transverse displacements of the sagbend are caused by pitch and surge motion of the lay-vessel, the maximum tangential displacements are caused by the pitch and surge motion as well and the maximum bending moment in the sagbend is induced by heave and surge motion of the lay-vessel. [7]

2.3. Finite Element Method

2.3.1. Theory

The Finite Element Method (FEM) is a numerical method for solving engineering problems. FEM is a widely spread method used by numerous industries facing different problems. Typical problem areas include structural analysis, heat transfer, fluid flow, mass transport, and electromagnetic potential. The laws of physics for these space- and time-dependent problems are usually expressed in terms of partial differential equations (PDEs). These PDEs cannot be solved analytically for the vast majority of these problems. To solve these PDEs an approximation of the equations is constructed, which is based upon different types of discretisations. These discretisations approximate the PDEs with numerical model equations, which can be solved using numerical methods. Because the numerical method is an approximation of the real situation, the solution to the numerical model is also an approximation of the real solution to the PDEs [6].

2.3.2. Flexcom

Flexcom is a non-linear FEM software package for the analysis of a wide range of compliant and rigid offshore structures [10]. It is used within HMC to analyse the installation of pipelines and risers both statically and dynamically. Flexcom uses a fourteen Degree of Freedom (DOF) hybrid beam finite element, the element has 6 DOFs at each node end and the axial force and torque are added to the usual three-dimensional beam element creating the fourteen DOFs in total. For the calculations of hydrodynamic forces in Flexcom the Morison equation is used. In Flexcom both the drag and inertia/added mass components of the Morison equation acting on the pipeline are based on the drag diameter (Dd), instead of the inertia and added terms being based on the displaced volume. The algorithms used within Flexcom for the discretisation of the finite element equations of motion in time are the Hilber-Hughes-Taylor integration and the Generalised-α method [10].

Morison equation

The Morison equation is a semi-empirical equation that calculates the hydrodynamic force over the length of a slender structure, a riser for example. The Morison equation for a fixed body in an oscillatory flow with velocity $u(t)$ is shown in equation 2.2 [4].

$$F(t) = \frac{\pi}{4}\rho C_M D^2 \cdot \dot{u}(t) + \frac{1}{2}\rho C_D D \cdot u(t)|u(t)| \tag{2.2}$$

Where:

- ρ : The density of the fluid [kg/m^3]
- C_D : Dimensionless drag coefficient [-]
- C_M : Dimensionless inertia coefficient [-]
- D : Diameter of the body. Originally the surface area A is used, but since $A = 1 \cdot D$ for a pipeline, D is used. [m]
- $F(t)$: Hydrodynamic force on the body per meter length [N/m]

This equation is the superposition of the drag in a current and the hydrodynamic inertia in an accelerating flow. The two force components are 90 degrees out of phase, this a direct consequence of the phase shift between velocity and acceleration of an oscillatory motion. The coefficients for drag, C_D, and inertia, C_M, are empirically determined, this can be done either analytically or numerically.

In case the body is not fixed but moves with velocity $v(t)$, the Morison equation changes to [8]:

$$F(t) = \underbrace{\rho\frac{\pi D^2}{4}\dot{u(t)}}_{a} + \underbrace{\rho C_a \frac{\pi D^2}{4}(\dot{u} - \dot{v})}_{b} + \underbrace{\frac{1}{2}\rho C_D D\,(u - v)\,|u - v|}_{c} \tag{2.3}$$

Where C_a is defined as the added mass coefficient related to the inertia coefficient as $C_M = C_a + 1$. Furthermore a, b and c are defined as:

a : Froude-Krylov force
b : Hydrodynamic mass force
c : Drag force

2.4. Dynamic substructuring

Divide et impera

Traiano Boccalini

This phrase has been attributed to King Philip II of Macedon, but there are many great leaders like Caesar and Napoleon who successfully applied this ancient technique on a wide range of domains. This technique of divide and conquer is at the basis of dynamic substructuring, because here likewise a complex problem is *divided* into smaller, simpler problems that are easier to overcome in order to *conquer* the whole problem.

2.4.1. Theory

The developments of the substructuring ideas came two decades after the development of the FEM. The desire of the engineers of those times to build better and bigger numerical models for more complex structures triggered this substructuring development, because the problem of these bigger models was that their size was limited by the computational power available. By dividing these bigger and more complex models into several smaller models of the global structure, so called substructures, the components dynamics could be obtained. With the use of these components dynamics, one could create compacter models of the global structure. There are two general methods of dynamic substructuring:

- Time-domain based substructuring
- Frequency-domain based substructuring

The time-domain based methods describe each subsystem by a generalized mass, damping and stiffness matrix. When the generalized substructure matrices are build using local modal properties one calls them

Component Mode Synthesis (CMS). The modal synthesis technique determines the dynamic behaviour of a coupled system on the basis of a normal mode description of the uncoupled systems. The most well known CMS technique is the Craig-Bampton method.
For the frequency domain based methods on the other hand, each subsystem is described in terms of Frequency Response Function (FRF) of the uncoupled systems. This method is named frequency based substructuring (FBS) [9]

2.4.2. Dynamic Stiffness Matrix

One frequency-domain based methods of substructuring is a Dynamic Stiffness Matrix. Because it is in the frequency domain, only linear approximations of the structures are analysed. In order to analyse the equation for the FBS, the dynamic Equation of Motion (EoM) has to be transferred into the frequency domain. The dynamic equation of motion in the time domain is given as:

$$\mathbf{M}\ddot{\mathbf{u}}(t) + \mathbf{C}\dot{\mathbf{u}}(t) + \mathbf{K}\mathbf{u}(t) = \mathbf{f}(t) \tag{2.4}$$

Transferring this equation with the use of the Fourier transform gives the dynamic equation of motion in the frequency domain:

$$\mathbf{Z}(\omega)\mathbf{u}(\omega) = \mathbf{f}(\omega) \quad \text{with} \quad \mathbf{Z}(\omega) = \left[-\omega^2\mathbf{M} + i\omega\mathbf{C} + \mathbf{K} \right] \tag{2.5}$$

The matrix $\mathbf{Z}(\omega)$ is referred to as the Dynamic Stiffness Matrix (DSM). The DSM consists of the complex-valued frequency-dependent functions that transfer the force required to generate a unit harmonic displacement at a certain DOF to the corresponding harmonic force response. The inverse of the matrix $\mathbf{Z}(\omega)$ is defined as the Flexibility Matrix, also known as the *receptance matrix* or *compliant stiffness* matrix, noted as $\mathbf{Y}(\omega)$:

$$\mathbf{u}(\omega) = \mathbf{Y}(\omega)\mathbf{f}(\omega) \tag{2.6}$$

The Flexibility Matrix $\mathbf{Y}(\omega)$ contains the frequency response functions of the structure that describe the displacement response to an harmonic input force.
There are numerous advantages of the FBS method ([2],[9]):

- It allows the evaluation of structures that would otherwise be too large and/or too complex to be simulated or measured as a whole. Or if not enough excitation energy can be put in the structure for adequate excitation.
- Experimentally obtained substructures (measurements) can be combined with numerical or analytical substructures, in order to compute the dynamic behaviour of the total structure. When experimental and theoretical models are combined, this is referred to as hybrid analysis.
- Local dynamic behaviour and its influence on the global behaviour can be determined more easily. This allows for local optimization of the design, but also for model simplification by eliminating local subsystem behaviour which has no significant impact on the assembled system.
- It allows for sharing and combining of substructures from different projects.
- When a substructure is changed, dynamic substructuring allows rapid evaluation of the dynamics of the complete system. Only the changed sub-part needs to be measured and thereby allows efficient local optimization, fast design cycles and subsequently an overall optimization.
- It allows easier spotting of local problems that might not be visible by testing the entire structure.

Of course there are disadvantages as well, the main disadvantages are ([2],[9]):

- Applicability of dynamic substructuring is usually limited to linear and stationary systems with constant parameters.
- For experimental substructuring, most measurements are limited to translational degrees of freedom because rotational degrees of freedom are difficult to measure. Assembling rotational DOFs is thus a major challenge.
- Dynamic substructuring code can take substantial time to program.
- For experimental substructuring, measurements containing noise are being used. The matrix inversions that are needed in the algorithms will propagate measurement noise, resulting in an inaccurate solution for the complete system.

2.4.3. Assembly of dynamic substructures

Substructures are structures that interact with their neighbouring structures. When two or more substructures are to be coupled, two conditions must always be satisfied, regardless of the coupling method used:

1. Compatibility of the substructures' displacements at the interface is the so-called compatibility condition.
2. Force equilibrium on the substructures' interface degrees of freedom is called the equilibrium condition.

For this thesis only the frequency domain is studied, so the following system in the frequency domain is considered. The governing equations are:

$$\mathbf{Z}(\omega)\mathbf{u}(\omega) = \mathbf{f}(\omega) + \mathbf{g}(\omega) \tag{2.7}$$

$$\mathbf{B}\mathbf{u}(\omega) = 0 \tag{2.8}$$

$$\mathbf{L}^T\mathbf{g}(\omega) = 0 \tag{2.9}$$

These equations describe the coupling between any number of substructures with any number of arbitrary couplings. Where **u** represents the complex amplitude of harmonic response, **f** the complex amplitude of harmonic external forces and **g** represents the the complex amplitude of harmonic connection forces. Finally **Z**, as defined in equation 2.5, is the diagonal matrix containing the dynamic stiffness matrices of the substructures. Furthermore equation 2.8 is the compatibility condition with the matrix **B** being a signed Boolean matrix, operating on the substructure interface DOF. The compatibility condition states that any pair of matching interface DOFs must have the same displacement, i.e. $u^k - u^l = 0$.
The equilibrium condition is defined by equation 2.9 where the matrix **L** is a Boolean matrix localizing the interface DOF of the substructures in the global set of DOF. This expression states that when the dual connection forces are summed, their resultant must be equal to zero, i.e. $g^k + g^l = 0$ [1].

Primal assembly in the frequency domain

In a primal formulation, a unique set of interface degrees of freedom is defined, and the interface forces are eliminated as unknowns using the interface equilibrium. Classically, finite element models are assembled in this primal manner. Mathematically, this is obtained by stating that:

$$\mathbf{u} = \mathbf{L}\mathbf{q} \tag{2.10}$$

where q is the unique set of interface DOF for the system.

Dual assembly in the frequency domain

In a dual assembly formulation, the full set of global DOF is retained, i.e., all interface DOF are present as many times as there are subdomains connected on the corresponding node. From equations 2.7 to 2.9, the dual assembled system is obtained by satisfying a priori the interface equilibrium. This is obtained by choosing the interface forces, also known as connection forces, in the form:

$$\mathbf{g} = -\mathbf{B}^T\lambda \tag{2.11}$$

Where λ are the Lagrange multipliers corresponding physically to the connection force intensities.

2.5. Linear response

In general dynamic problems can be classified into either linear problems or non-linear problems, depending on material constitutive law and assumptions about deformations and displacement. Mathematically, a system is defined as linear if the relationship between the input signal and the output signal obeys the following conditions [5]:

- *Principle of superposition*
  According to this principle, if an input signal $\alpha(t)$ gives rise to an output signal $\beta(t)$, and an input signal $\gamma(t)$ gives rise to an output signal $\delta(t)$. Then the input signal $\alpha(t) + \gamma(t)$ gives an output signal equal to $\beta(t) + \delta(t)$.
- *Principle of homogeneity*
  A system is said to obey the principle of homogeneity if output of the function $\alpha(t)$ with the input multiplied with scalar λ is equal to the output of the same function $\alpha(t)$ multiplied by the scalar λ, i.e. $\alpha(\lambda \cdot t) = \lambda \cdot \alpha(t)$.

- *Frequency Conservation*
  A system is said to be frequency conserving if the frequency content present in the input signal also exists in the output signal.

Linear perturbations

A problem with small perturbations and a linear elastic material is classified as linear. This can be proven with the use of the Taylor series, equation 2.12

$$f(x) = f(a) + \frac{f'(a)}{1!}(x-a) + \frac{f''(a)}{2!}(x-a)^2 + \frac{f'''(a)}{3!}(x-a)^3 + \cdots + \frac{f^{(n)}(a)}{n!}(x-a)^n \tag{2.12}$$

For clarification the following equation of motion is taken as an example.

$$\frac{d^2x}{dt^2} + \sin(\theta_0 + x) = 0 \tag{2.13}$$

Now apply the Taylor series expansion to the non-linear part of this equation which results in:

$$\sin(\theta_0 + x) = \sin\theta_0 + x\cos\theta_0 - \frac{1}{2}x^2\sin\theta_0 \cdots + x^n\frac{1}{n!}\sin\theta_0 \tag{2.14}$$

For small perturbations it is assumed that $x \ll 1$, it can be assumed that $x^n \ll x$ and so only the linear part remains:

$$\sin(\theta_0 + x) = \sin\theta_0 + x\cos\theta_0 \tag{2.15}$$

2.6. Scope

In order to make this research manageable a scope is defined. The scope consists of the properties of the pipeline that is studied and the assumptions regarding the environmental influences and loading scenarios. Both are discussed in the subsections below.

2.6.1. Pipeline properties

A large variety of pipelines exists, which pipeline is used, depends on the project. Each project requires its specific pipeline properties. For this research the properties of the tender project *Liza* were chosen.

Case for this research: Liza project

The Liza field is one of the largest oil discoveries of the past decade and located off the coast of Guyana in South America. The field is part of the Stabroek Block, which measures 26,800 square kilometres. The Liza field is approximately 190 kilometres offshore in water depths of 1,500 to 1,900 meters. In table 2.1 a summary of the properties that were used for this research is shown.

Table 2.1: Pipeline properties used for research

Property	**Value**	**Unit**
Water depth	1,850	m
OOD	18.75	inch
OD	12.75	inch
WT	33.00	mm

2.6.2. Assumptions

Assumptions are made to reduce the amount of variables of the problem and focus on the core of the problem of this research. Below is a list of assumptions and some further explanation to some of these assumptions to clarify them.

- 3 DOFs in plane motion: only translation in X- and Y-direction and rotation around Z. See figure 1 on page xi for axis convention.
- No residual stresses in the pipeline.
- Twist in the pipeline is neglected.
- The seabed is flat and interaction with the soil is stiff.
- The installation method used is the J-lay method.
- No out of plane bending of the pipeline.
- Pipeline is not flooded, i.e. filled with air.
- Small perturbations around geometric nonlinear (GNL) equilibrium are assumed to be linear as explained in section 2.5.tf

3

Methodology

3.1. Current methodology of HMC

Currently, the dynamic FEM assessment of the sagbend is not being performed in detail within HMC. The current practice is as follows: with the software package Flexcom, a global model of the pipeline installation is dynamically assessed. From this assessment all the loads are obtained, but since at HMC Flexcom is only used within the elastic limit, no failures are modelled with this assessment. Therefore an additional FEM assessment is needed. This additional assessment is a local assessment of the cut-out of the sagbend with the use of the Abaqus software. In contrast with the global assessment, this local assessment is done statically. The local sagbend model is loaded with the maximum bending moments obtained from the dynamic Flexcom assessment. It is then checked if the result of this static assessment does not exceed the design standards set by the DNV.

3.1.1. Advantages and drawbacks of current methodology

Advantages

- Quicker than a time dependent assessment with Abaqus.
- Safe (over)estimation of loads.

Drawbacks

- This method is a conservative method.
- No fatigue assessment possible.
- Interface issues occur when transferring data between software packages.

3.2. Enhanced methodology

As mentioned in chapter 1 the objective of this research is to improve the efficiency of the current method(3.1), while maintaining robust and reliable. Performing the Abaqus FEM assessment with time-varying bending moments calculated in the global Flexcom model would already be an improvement on the reliability of the results, it would however not be more efficient. It would be very time consuming to perform time dependent runs for each load case scenario, which creates the necessity for another method. The enhanced method that could improve on all three objectives is a methodology that makes use of a DSM, which was already mentioned in step 3 and 4 and shown in figure 1.5 in chapter 1. The enhanced methodology exists of 6 Phases which are explained on the next pages.

Phase 1: Global model in Flexcom

The first phase is to construct a global model of the installation scenario that is to be investigated, in this case the Liza tender project. The properties of this project are listed in 2.1. The global model is constructed with the use of the Flexcom software. The global model in the Flexcom software is shown in figure 3.1.

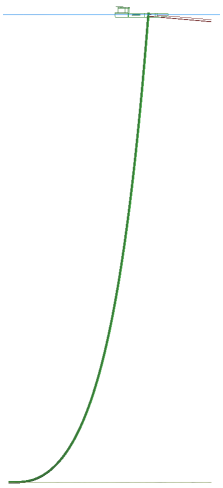

Figure 3.1: Global model in Flexcom

Phase 2: Cut-out the sagbend

The second phase consists of determining the sagbend region. The sagbend region is chosen as such that the node of the pipeline with the highest fatigue damage is accounted for in the sagbend. Thereafter this sagbend region is removed from the global model. At the cut-off points the static reaction forces are determined. The catenary shape of the remaining part of the global model is maintained with these static reaction forces , see figure 3.2.

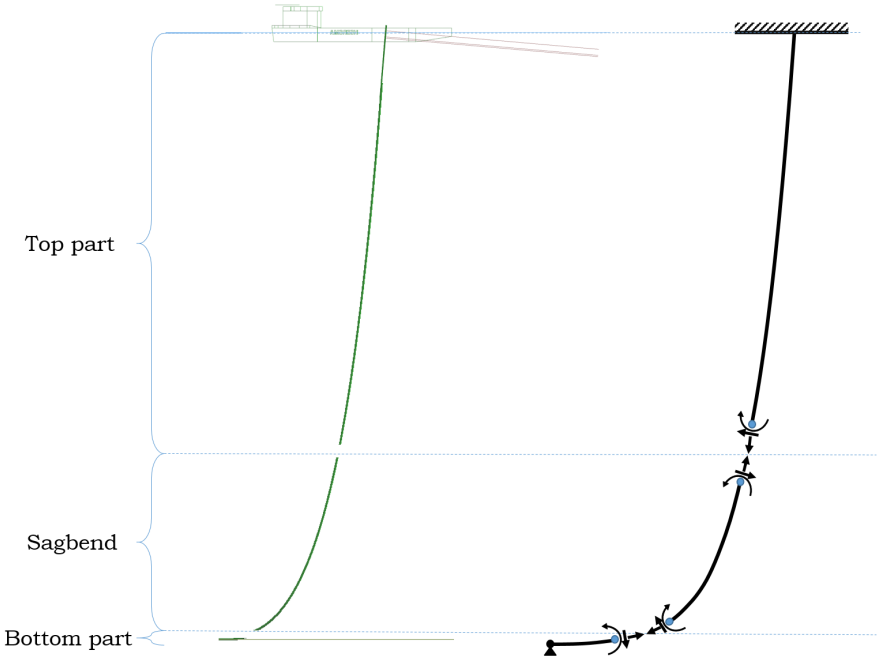

Figure 3.2: Free body diagram of the global model in Flexcom

Phase 3: Force excitation of the remaining parts of the global model

The remaining part of the global model shown in figure 3.2 is divided in a top part, consisting of the vessel and free hanging pipeline, and a bottom part, consisting of the pipeline at the seabed. It is assumed that the pipeline is clamped at the vessel and at the bottom end the pipeline is hinged. Thereafter both the bottom and top part are excited by a harmonic force. This is done separately, but the procedure is the same for both parts, as is shown in figures 3.3a and 3.3b.

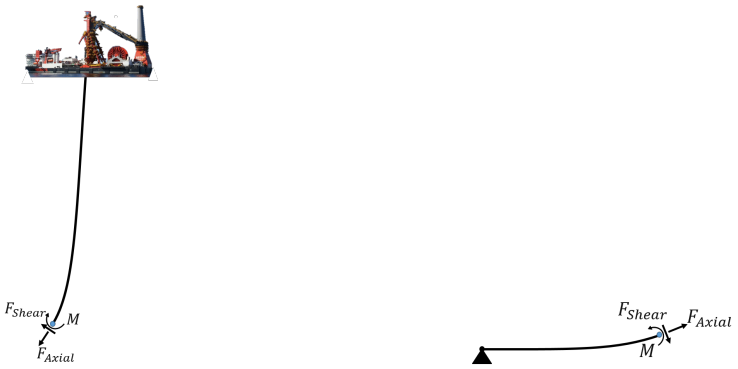

(a) Excitation of the top part

(b) Excitation of the bottom part

Figure 3.3: Excitation of the remaining parts of the global model

The excitation is done by applying a harmonic force with a certain amplitude on top of the static equilibrium forces. This harmonic force is applied on the cut-off point of a remaining part. The Flexcom software does not compute imaginary numbers, so the $\cos(\Omega t)$ is used, resulting in equation 3.1.

$$\mathbf{F} = \begin{bmatrix} F_{Axial} \cdot \cos(\Omega t) \\ F_{Shear} \cdot \cos(\Omega t) \\ M \cdot \cos(\Omega t) \end{bmatrix} \tag{3.1}$$

Each force DOF is applied separately, creating three force vectors, shown in equation 3.2.

$$\mathbf{F} = \begin{bmatrix} F_{Axial} \cdot \cos(\Omega t) \\ 0 \cdot \cos(\Omega t) \\ 0 \cdot \cos(\Omega t) \end{bmatrix}; \quad \mathbf{F} = \begin{bmatrix} 0 \cdot \cos(\Omega t) \\ F_{Shear} \cdot \cos(\Omega t) \\ 0 \cdot \cos(\Omega t) \end{bmatrix}; \quad \mathbf{F} = \begin{bmatrix} 0 \cdot \cos(\Omega t) \\ 0 \cdot \cos(\Omega t) \\ M \cdot \cos(\Omega t) \end{bmatrix} \tag{3.2}$$

For each force DOF the displacement in all three DOF is captured in the vector **u** containing the tangential displacement u, the transverse displacement w and the rotation ϕ. Note that the orientation of the local axis is based on the static configuration and does not follow the deformed shape. A graphic representation of the excitation procedure for a simple beam model is shown in figure 3.4.

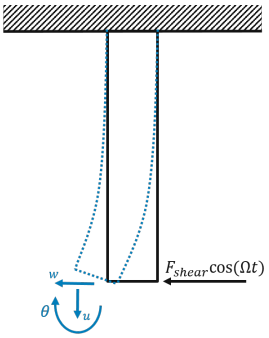

Figure 3.4: Example of shear force excitation procedure

After the system has been excited by all 3 force DOFs a total of 9 displacement responses is recorded. The post-processing of these responses is explained in Phase 4.

Phase 4: Calculate the DSM

As was mentioned in the section Phase 3, 9 displacement responses are recorded. An example of possible responses for a simple beam is shown below in figure 3.5.

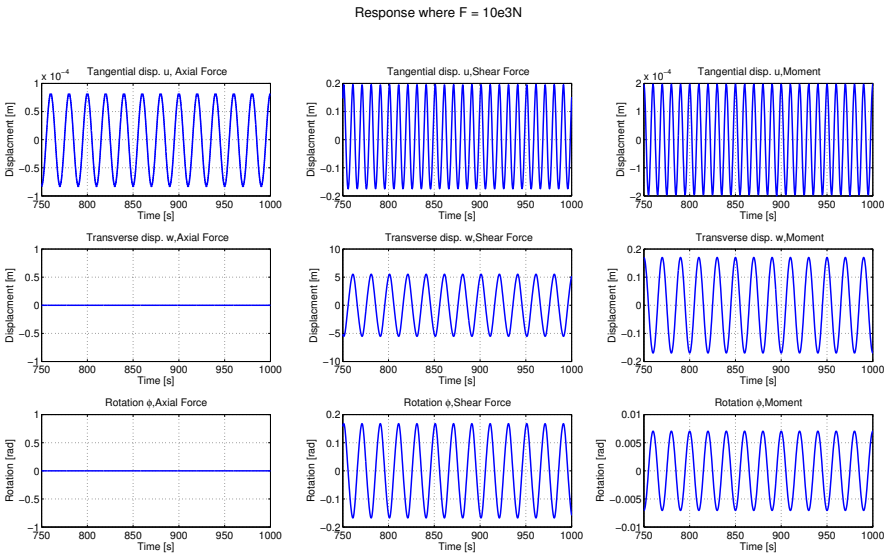

Figure 3.5: Example of displacement responses

The positioning of the 9 responses in the matrix is defined as listed below and shown in figure 3.6:

1.1 The tangential response caused by the axial force: Top-Left in 3.5 & 3.6
1.2 The tangential response caused by the shear force: Top-Middle in 3.5 & 3.6
1.3 The tangential response caused by the moment: Top-Right in 3.5 & 3.6
2.1 The transverse response caused by the axial force: Middle-Left in 3.5 & 3.6
2.2 The transverse response caused by the shear force: Middle-Middle in 3.5 & 3.6
2.3 The transverse response caused by the moment: Middle-Right in 3.5 & 3.6
3.1 The rotational response caused by the axial force: Bottom-Left in 3.5 & 3.6
3.2 The rotational response caused by the shear force: Bottom-Middle in 3.5 & 3.6
3.3 The rotational response caused by the moment: Bottom-Right in 3.5 & 3.6

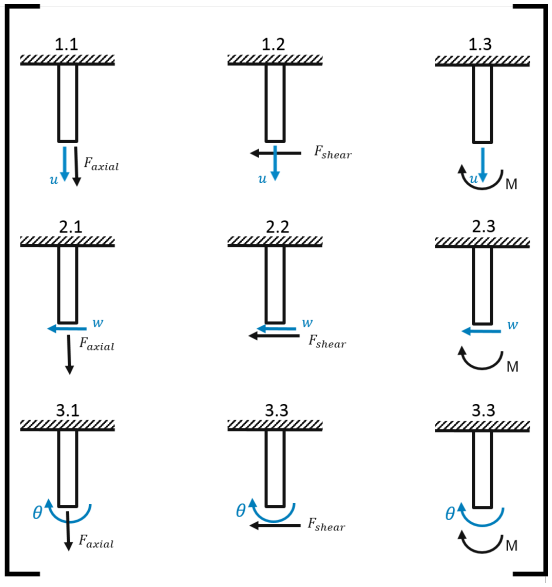

Figure 3.6: Sign convention for the matrices. Where blue arrows=displacement and black arrows=force

The dynamic stiffness can be calculated with these displacement responses and the excitation forces. As stated in chapter 1 this is defined as the ratio $DSM(\Omega) = \frac{\mathbf{F}(\Omega)}{\mathbf{u}(\Omega)}$. Since the system is excited by a harmonic force, the Flexibility Matrix, which is the inverse of the DSM, is calculated first. This is done for each of the 9 entries of the matrix. In order to perform the calculations, first the displacement responses and the harmonic forces need to be transferred from time traces to frequency spectra with the use of the Fast Fourier Transform (FFT). The maxima of the spectra at the excitation frequency (Ω_{ex}) are used as the input for the ratio calculations. Note that these numbers will be complex valued. The calculation procedure of the Flexibility Matrix is shown in equation 3.3.

$$\textbf{Flexibility Matrix}(\Omega = \Omega_{ex}) = \begin{bmatrix} \frac{u(\Omega)}{F_{Axial}(\Omega=\Omega_{ex})} & \frac{u(\Omega=\Omega_{ex})}{F_{Shear}(\Omega=\Omega_{ex})} & \frac{u(\Omega=\Omega_{ex})}{M(\Omega=\Omega_{ex})} \\ \frac{w(\Omega=\Omega_{ex})}{F_{Axial}(\Omega=\Omega_{ex})} & \frac{w(\Omega=\Omega_{ex})}{F_{Shear}(\Omega=\Omega_{ex})} & \frac{w(\Omega=\Omega_{ex})}{M(\Omega=\Omega_{ex})} \\ \frac{\phi(\Omega=\Omega_{ex})}{F_{Axial}(\Omega=\Omega_{ex})} & \frac{\phi(\Omega=\Omega_{ex})}{F_{Shear}(\Omega=\Omega_{ex})} & \frac{\phi(\Omega=\Omega_{ex})}{M(\Omega=\Omega_{ex})} \end{bmatrix} \tag{3.3}$$

The above shown calculation method gives the 3x3 Flexibility Matrix with complex valued numbers. Taking the inverse of this matrix results in the 3x3 DSM, also with complex valued numbers. Completing these calculations steps for both the top and the bottom part results in two DSMs. These DSMs comprise all the information of the remaining structure above and below the sagbend and can be used as dynamic boundary conditions, see figure 3.7.

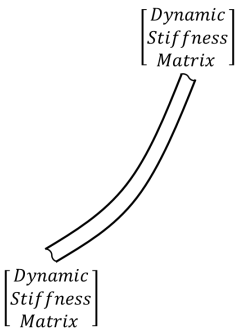

Figure 3.7: Sagbend with DSM as boundary conditions

Moreover it should be mentioned, that this DSM can only be calculated for linear or approximately linear systems. Consequently the DSM must be symmetric. This requirement is used to check whether the DSM is correct.

Phase 5: Determine critical period with SpeRA-tool

SpeRa refers to Spectral Response Analysis and represents a tool that was developed within HMC to compute responses of a non-linear system in the frequency domain based on Response Amplitude Operators (RAOs) derived using a white noise wave spectrum. The initial objective was to assess the critical period for a pipelay system, the main objective however is to get more insight on the behaviour of the pipelay system. The analysis methodology of SpeRA is to perform a time domain simulation using a white noise wave spectrum. The results of this simulation are transformed into the frequency domain using a FFT algorithm after which the spectral response is derived. The final output of the analysis is a RAO for the output parameter of interest. This is graphically shown in 3.8.

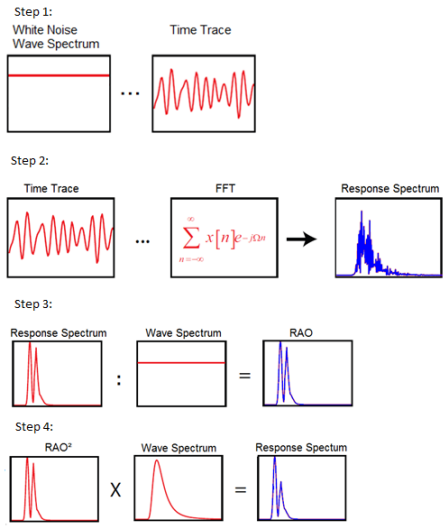

Figure 3.8: Steps performed by SpeRA tool

With this SpeRA tool the critical period for the sagbend is obtained. This critical period is then used for the harmonic excitation of the global model. From this dynamic assessment of the global model the internal forces at the cut-off nodes are obtained. These internal forces are then applied to the local model.

Phase 6: Detailed FEM assessment with the Abaqus software package

The final phase of the enhanced method is to use the output generated by the previous phases to perform a detailed dynamic FEM assessment of the sagbend. First a local FEM model of the sagbend needs to be constructed in the Abaqus software with all the properties and external forces (e.g. hydrodynamic). At the boundaries of the global model, the DSMs for $\Omega = \Omega_{ex}$ and the connection forces are imposed on the system as boundary conditions. Thereafter, this local FEM model is combined with the force output from the global model to assess the sagbend segment, this combination is graphically shown in figure 3.9.

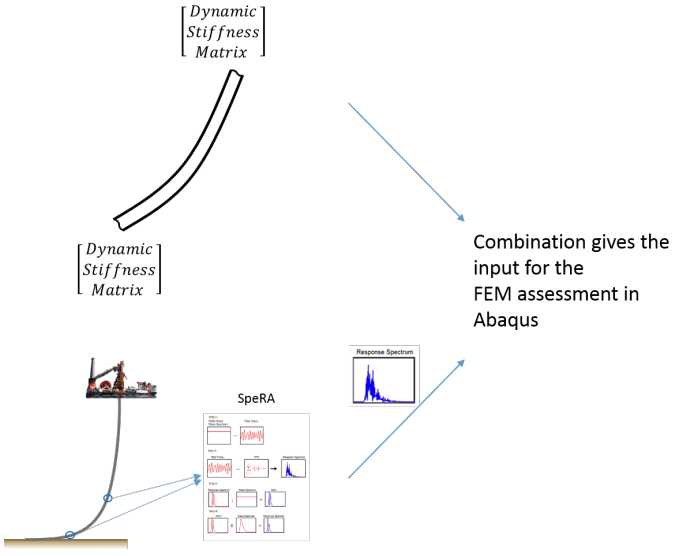

Figure 3.9: Combination of the DSM and SpeRA output

Ultimately the model used for this assessment is a local FEM model and could include another component in the sagbend such as a counterbore or a collar. An example of an Abaqus FEM model of the sagbend is shown in figure 3.10.

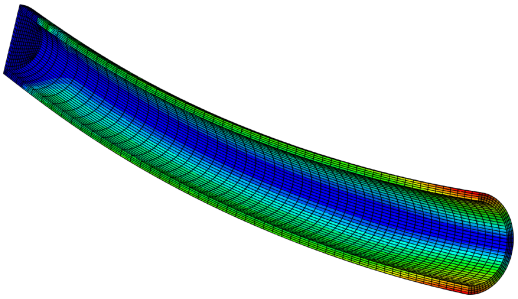

Figure 3.10: Example of sagbend FEM model in Abaqus

3.2.1. Advantages and drawbacks of the enhanced methodology

Advantages

- The enhanced methodology gives more accurate load estimation than current methodology.
- This methodology is quicker than conventional dynamic assessments.
- In the local model small property changes can be made to perform different analyses. This does allowed if these changes do not drastically influencing the global behaviour.
- Allows for combination of several FEM models.
- Allows for combination with measured or experimental data.

Drawbacks

- The application of this method is not proven for pipelines.
- The responses at the cut-off locations are linearised.
- Time-consuming to construct the dynamic substructuring code. Construction of the DSMs and subroutines is a time consuming endeavour.

But before this enhanced method can be applied to an actual pipeline, the methodology was tested on more simpler models to verify its feasibility. This is shown in chapter 4.

4

Model

4.1. Step 1: Demonstration of an analytical equivalent with a cut-out segment

In this section the analytical model is explained and demonstrated. It is however important to clearly state the sign convention of the forces. This sign convention is shown in figure 4.1.

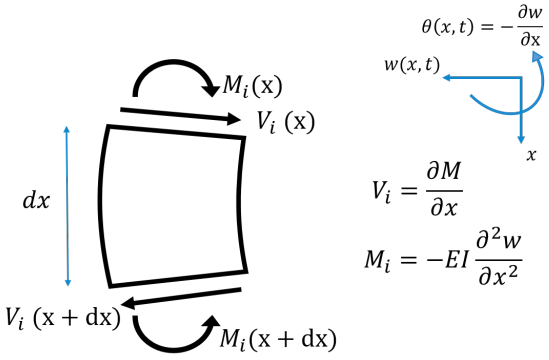

Figure 4.1: Sign convention of the internal forces

Furthermore, this section is divided into four subsection. The first subsection is the global model of the analytical model, the second subsection is DSM calculation, the third is the local model and finally the last subsection regarding the demonstration with numerical values.

4.1.1. Global model

To mimic the situation of a pipeline during installation, another slightly different analytical model was used. A vertical Bernoulli beam, hinged on both ends and with distributed dash-pots was used for this model. However the top part is now harmonically displaced to simulate vessel motions, as is shown in figure 4.2.

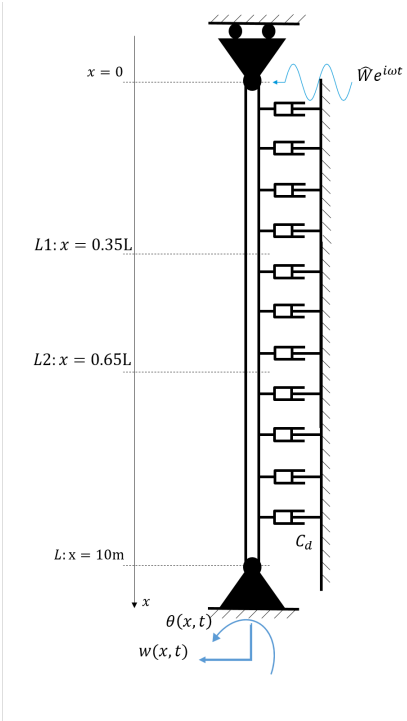

Figure 4.2: Analytical equivalent vertical: Global model

For the global model of this analytical equivalent the following equation of motion was used:

$$\rho A \frac{\partial^2 w}{\partial t^2} + EI \frac{\partial^4 w}{\partial x^4} + c_d \frac{\partial w}{\partial t} = 0 \tag{4.1}$$

With the boundary conditions as stated below:

- $x = 0$
  - $w(0,t) = \hat{W} e^{i\omega t}$
  - $\frac{\partial^2 w(0,t)}{\partial x^2} = 0$
- $x = L$
  - $w(L,t) = \frac{\partial^2 w(L,t)}{\partial x^2} = 0$

Solving the equation of motion in the frequency domain, using $W(x)e^{i\omega t}$, combined with the the boundary conditions, gives an expression for the displacement of the global model, $W_{global}(x)$, including the coefficients. This is shown in equation 4.2.

$$W_{global}(x) = \frac{\hat{W} \cdot \cosh(\beta x)}{2} - \frac{\hat{W} \cdot \cosh(\beta L)\sinh(\beta x)}{2\sinh(\beta L)} + \frac{\hat{W} \cdot \cos(\beta x)}{2} - \frac{\hat{W} \cdot \cos(\beta L)\sin(\beta x)}{2\sin(\beta L)} \tag{4.2}$$

With β defined as:

$$\beta^4 = \frac{\rho A \omega^2 - i\omega c_d}{EI}$$

When the x in equation 4.2 is replaced by L_1 and L_2, the displacement amplitudes of these points are obtained. These displacements are ultimately compared to the displacements of the same points but calculated with the expression for the displacement of the local cut-out model.

4.1.2. DSM model

Top part

A cut is made at $x = L_1$ for the calculation of the DSM of the top part. The equation of motion remains the same as the one in equation 4.1. A schematic representation of this model is shown in figure 4.3.

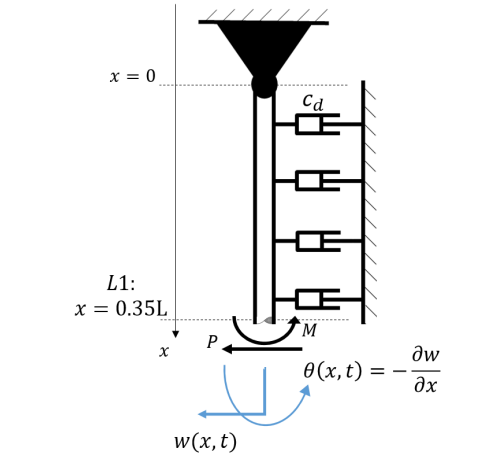

Figure 4.3: Analytical equivalent: DSM model

At $x = L_1$, where the cut is made, a force and a moment are applied in the positive force direction, as is shown in figure 4.3. This force and moment should be equal to the displacement and rotation multiplied with the Dynamic Stiffness Matrix, as is shown in equation 4.3.

$$\begin{bmatrix} P \\ M \end{bmatrix} = \begin{bmatrix} DSM_{1,1} & DSM_{1,2} \\ DSM_{2,1} & DSM_{2,2} \end{bmatrix} \begin{bmatrix} w \\ \theta \end{bmatrix} \tag{4.3}$$

The values of the DSM are found by solving the system of the top part twice. For each calculation the boundary conditions at the free end ($x = L_1$) are different.

Step 1): For the first calculation, it is assumed that the end ($x = L_1$) is displaced by 1 meter and that the rotation is zero, resulting in the following boundary conditions:

At $x = 0$:

- $w(0,t) = 0$
- $\frac{\partial^2 w(0,t)}{\partial x^2} = 0$

At $x = L_1$

- $w(L_1,t) = 1$
- $\theta(L_1,t) = 0$

Solving the system for these boundary conditions results in an expression for $W(x)$, let's call this $W_1(x)$. This expression is then used to calculate a part of the DSM for the top part. This is done by solving the equilibrium conditions at $x = L_1$, that are shown in figure 4.4.

(a) Force equilibrium

(b) Moment equilibrium

Figure 4.4: Equilibrium condition at $x = L_1$ for a element with size dx

Where P and M are the external force and moment, and V_i and M_i are the internal force and moment. These equilibrium conditions combined with the DSM in equation 4.3, result in the following expressions for $DSM_{1,1}$ and $DSM_{2,1}$:

$$DSM_{1,1}|_{L_1} = P = V_i|_{L_1} = -EI\frac{\partial^3 W_1(L_1)}{\partial x^3} \tag{4.4}$$

$$DSM_{2,1}|_{L_1} = M = M_i|_{L_1} = -EI\frac{\partial^2 W_1(L_1)}{\partial x^2} \tag{4.5}$$

Note that $DSM_{1,1} = P$ and $DSM_{2,1} = M$ comes from equation 4.3 with $w = 1$ and $\theta = 0$.

Step 2): For the second calculation, it is assumed that at the end ($x = L_1$) now the displacement is zero and that the end is rotated by 1 radian, resulting in the following boundary conditions:

At $x = 0$

- $w(0,t) = 0$
- $\frac{\partial^2 w(0,t)}{\partial x^2} = 0$

At $x = L_1$

- $w(L_1,t) = 0$
- $\theta(L_1,t) = 1$

When the system is solved with these boundary conditions a different expression for $W(x)$ is found, let's call this one $W_2(x)$. This expression is used to calculate the remaining unknown parts of the DSM; $DSM_{1,2}$ and $DSM_{2,2}$. Again these equilibrium conditions of figure 4.4 are combined with the DSM in equation 4.3. This results in the following expressions for $DSM_{1,2}$ and $DSM_{2,2}$:

$$DSM_{1,2}|_{L_1} = P = V_i|_{L_1} = -EI\frac{\partial^3 W_2(L_1)}{\partial x^3} \tag{4.6}$$

$$DSM_{2,2}|_{L_1} = M = M_i|_{L_1} = -EI\frac{\partial^2 W_2(L_1)}{\partial x^2} \tag{4.7}$$

Note that $DSM_{1,2} = P$ and $DSM_{2,2} = M$ comes from equation 4.3 with $w = 0$ and $\theta = 1$.
The complete DSM of the top part at $x = L1$ is now known using the two aforementioned calculations steps.

Lower part

Now that the DSM for the top part is known, the calculation steps can be repeated on the lower part of the model, which is shown in figure 4.5.

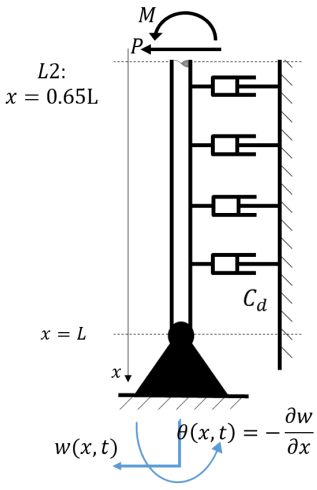

Figure 4.5: Analytical equivalent: DSM model of the lower part

The procedure is identical to that of the top part. The difference is in the force and moment equilibrium, which are shown in figure 4.6.

(a) Force equilibrium (b) Moment equilibrium

Figure 4.6: Equilibrium condition at $x = L_2$ for a element with size dx

With the force and moment equilibrium of figure 4.6 and the equation 4.3 the expression for the DSM of the lower part is calculated in the aforementioned two steps, which are repeated in short below:

Step 1: For step 1 of the lower part, the boundary conditions are defined as shown below. Solving the system of the lower part for these boundary conditions results in a new $W_1(x)$ for the bottom part.

At $x = 0$

- $w(L,t) = 0$
- $\frac{\partial^2 w(L,t)}{\partial x^2} = 0$

At $x = L_1$

- $w(L_2,t) = 1$
- $\theta(L_2,t) = 0$

With this expression $W_1(x)$ the expressions for the DSM are found:

$$DSM_{1,1}|_{L_2} = P = -V_i|_{L_2} = EI\frac{\partial^3 W_1(L_2)}{\partial x^3} \tag{4.8}$$

$$DSM_{2,1}|_{L_2} = M = -M_i|_{L_2} = EI\frac{\partial^2 W_1(L_2)}{\partial x^2} \tag{4.9}$$

Step 2: Then for step 2 the following boundary conditions hold:

At $x = 0$

- $w(L,t) = 0$
- $\frac{\partial^2 w(L,t)}{\partial x^2} = 0$

At $x = L_1$

- $w(L_2,t) = 0$
- $\theta(L_2,t) = 1$

These boundary conditions result in a new expression $W_2(x)$ for the bottom part, with which the remaining unknowns of the DSM of the bottom part are found:

$$DSM_{1,2}|_{L_2} = P = -V_i|_{L_2} = EI\frac{\partial^3 W_2(L_2)}{\partial x^3} \tag{4.10}$$

$$DSM_{2,2}|_{L_2} = M = -M_i|_{L_2} = EI\frac{\partial^2 W_2(L_2)}{\partial x^2} \tag{4.11}$$

Note that $W_1(x)$ and $W_2(x)$ are different expressions for the top and bottom part.
With the two steps the complete expression for the DSM for the bottom part of the global model is obtained. The next step is to assemble the two DSMs and the local model, now that the expressions for both of the DSMs are known.

4.1.3. Assembly of Cut-out segment and DSMs

As stated before, the final step is to bring the local model of the cut-out together with the DSMs. A schematic representation of this local model is shown in figure 4.7.

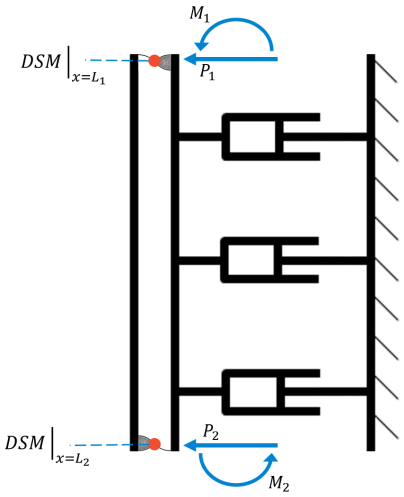

Figure 4.7: Analytical equivalent vertical: Local model

Connection forces and moments are required for this assembly, as was explained in subsection 2.4.3. To determine these connections forces, the force and moment equilibria need to be constructed for both ends of the local model.

Resulting in the following equilibria:

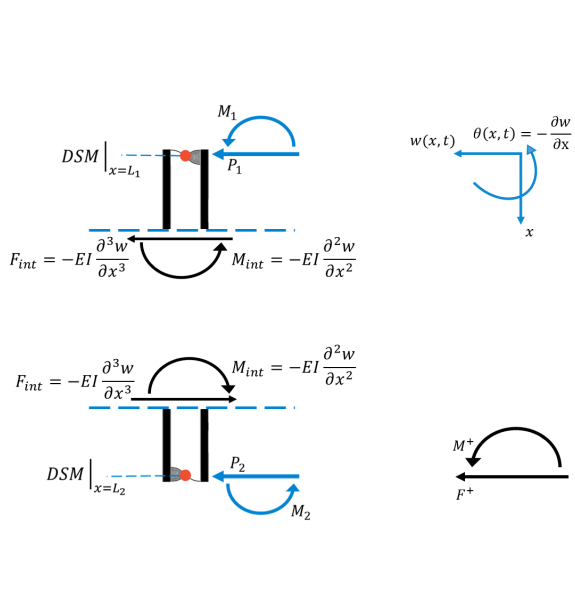

Figure 4.8: Free body diagram of the local model

- at $x = L_1$, the $\sum$F and $\sum$ M are:
  - $P_1 - DSM_{1,1}\big|_{x=L_1} \cdot w - DSM_{1,2}\big|_{x=L_1} \cdot \theta + (-EI\frac{\partial^3 w}{\partial x^3}) = 0$
  - $M_1 - DSM_{2,1}\big|_{x=L_1} \cdot w - DSM_{2,2}\big|_{x=L_1} \cdot \theta + (-EI\frac{\partial^2 w}{\partial x^2}) = 0$
- at $x = L_2$, the $\sum$F and $\sum$ M are:
  - $P_1 - DSM_{1,1}\big|_{x=L_2} \cdot w - DSM_{1,2}\big|_{x=L_2} \cdot \theta - (-EI\frac{\partial^3 w}{\partial x^3}) = 0$
  - $M_1 - DSM_{2,1}\big|_{x=L_2} \cdot w - DSM_{2,2}\big|_{x=L_2} \cdot \theta - (-EI\frac{\partial^2 w}{\partial x^2}) = 0$

The connection forces and moments at both ends are then calculated using the force and the moment equilibria shown in figure 4.8 and the equations next the it. This results in the connections loads are depicted as a formula in equations 4.12 and 4.13.

$$\begin{bmatrix} P_1 \\ M_1 \end{bmatrix} = \begin{bmatrix} DSM_{1,1}|_{x=L_1} & , & DSM_{1,2}|_{x=L_1} \\ DSM_{2,1}|_{x=L_1} & , & DSM_{2,2}|_{x=L_1} \end{bmatrix} \begin{bmatrix} W_{global}(x=L_1) \\ \theta_{global}(x=L_1) \end{bmatrix} - \begin{bmatrix} -EI\frac{\partial^3 W_{global}(x=L_1)}{\partial x^3} \\ -EI\frac{\partial^2 W_{global}(x=L_1)}{\partial x^2} \end{bmatrix} \tag{4.12}$$

$$\begin{bmatrix} P_2 \\ M_2 \end{bmatrix} = \begin{bmatrix} DSM_{1,1}|_{x=L_2} & , & DSM_{1,2}|_{x=L_2} \\ DSM_{2,1}|_{x=L_2} & , & DSM_{2,2}|_{x=L_2} \end{bmatrix} \begin{bmatrix} W_{global}(x=L_2) \\ \theta_{global}(x=L_2) \end{bmatrix} + \begin{bmatrix} -EI\frac{\partial^3 W_{global}(x=L_2)}{\partial x^3} \\ -EI\frac{\partial^2 W_{global}(x=L_2)}{\partial x^2} \end{bmatrix} \tag{4.13}$$

Now that the values of the connection loads at both boundaries are known, the boundary conditions of the local model can be formulated. These boundary conditions are required for the calculation of the displacement of the local model W_{local}. Where the expression of the local displacement is shown in equation 4.14 and the boundary conditions are shown in equations 4.15 and 4.16.

$$W_{local}(x) = B_1 \cdot \cosh(\beta x) + B_2 \cdot \sinh(\beta x) + B_3 \cdot \cos(\beta x) + B_4 \cdot \sin(\beta x) \tag{4.14}$$

$$\begin{bmatrix} P_1 \\ M_1 \end{bmatrix} = \begin{bmatrix} DSM_{1,1}|_{x=L_1} & , & DSM_{1,2}|_{x=L_1} \\ DSM_{2,1}|_{x=L_1} & , & DSM_{2,2}|_{x=L_1} \end{bmatrix} \begin{bmatrix} W_{local}(x=L_1) \\ \theta_{local}(x=L_1) \end{bmatrix} - \begin{bmatrix} -EI\frac{\partial^3 W_{local}(x=L_1)}{\partial x^3} \\ -EI\frac{\partial^2 W_{local}(x=L_1)}{\partial x^2} \end{bmatrix} \tag{4.15}$$

$$\begin{bmatrix} P_2 \\ M_2 \end{bmatrix} = \begin{bmatrix} DSM_{1,1}|_{x=L_2} & , & DSM_{1,2}|_{x=L_2} \\ DSM_{2,1}|_{x=L_2} & , & DSM_{2,2}|_{x=L_2} \end{bmatrix} \begin{bmatrix} W_{local}(x=L_2) \\ \theta_{local}(x=L_2) \end{bmatrix} + \begin{bmatrix} -EI\frac{\partial^3 W_{local}(x=L_2)}{\partial x^3} \\ -EI\frac{\partial^2 W_{local}(x=L_2)}{\partial x^2} \end{bmatrix} \tag{4.16}$$

Because the connection forces P_1, P_2, M_1 and M_2 are known from equations 4.12 and 4.13, the boundary conditions in equation 4.15 and 4.16 result in four equations with four unknowns. These four unknowns are the coefficients $\sum_{i=1}^{4} B_i$ of 4.14, solving this system results in the values of $\sum_{i=1}^{4} B_i$ and thus the symbolic expression of $W_{local}(x)$.

4.1.4. Result of analytical cut-out segment

The symbolic expressions of the displacement of the global model as well as the displacement of the local model are now known. In order to verify whether the displacements at the cut-off boundaries are identical the following parameters were used:

- EI $= 6.489 \cdot 10^5$ [Nm^2]
- $\rho = 7800$ [kg/m^3]
- A $= 0.0391$ [m^2]
- $L = 10$ [m]
- $L_1 = 0.35 \cdot L$ [m]
- $L_2 = 0.65 \cdot L$ [m]
- $\omega = 0.2\pi$ [rad/s]
- $\hat{W} = 1$ [m]
- $c_d = 1 \cdot 10^4$ [kg/s]

The numerical values of the DSMs can be calculated using these parameters. This results in the following DSMs:

$$DSM|_{x=L_1} = \begin{bmatrix} 45235.49 + 10682.58i & 158819.52 + 6598.36i \\ 158819.52 + 6598.36i & 556129.64 + 5132.17i \end{bmatrix} \tag{4.17}$$

$$DSM|_{x=L_2} = \begin{bmatrix} 45235.49 + 10682.58i & -158819.52 - 6598.36i \\ -158819.52 - 6598.36i & 556129.64 + 5132.15i \end{bmatrix} \tag{4.18}$$

By inserting these DSMs into equations 4.12 and 4.13, the connection forces become:

$$\begin{aligned} P_1 &= (45439.44 - 3063.80i) \cdot e^{i\omega t} \text{ N} \\ M_1 &= (158951.19 - 3024.46i) \cdot e^{i\omega t} \text{ Nm} \\ P_2 &= (-0.000255 + 0.000098i) \cdot e^{i\omega t} \text{ N} \\ M_2 &= (0.00048 - 0.00023i) \cdot e^{i\omega t} \text{ Nm} \end{aligned}$$

The above shown values of P_1, M_1, P_2 and M_2 are also used to verify the DSMs. Since the value of the connection force should be zero, if there is no external force present beyond the location of that specific connection force. There is a external force present for the connection forces P_1 and M_1, so these are non-zero. Below the location of P_2 and M_2 however no external force is present, and these should be zero, since this is the case the DSMs are considered to be correct.

With the numerical values of both the DSMs, P_1, M_1, P_2 and M_2, the dynamic substructuring method can be verified. For the verification of the analytical approach two snapshots are displayed in figures 4.9 and 4.10. Where in figure 4.9 the shape of the beam between $x = L_1$ and $x = L_2$ at $t = 17$ seconds caused by the real part of the excitation is shown and in figure 4.10 the shape caused by the imaginary part of the excitation is shown. From these results it is concluded that the dynamic substructuring method works for analytical models and is a quick and efficient method of analysing local models.

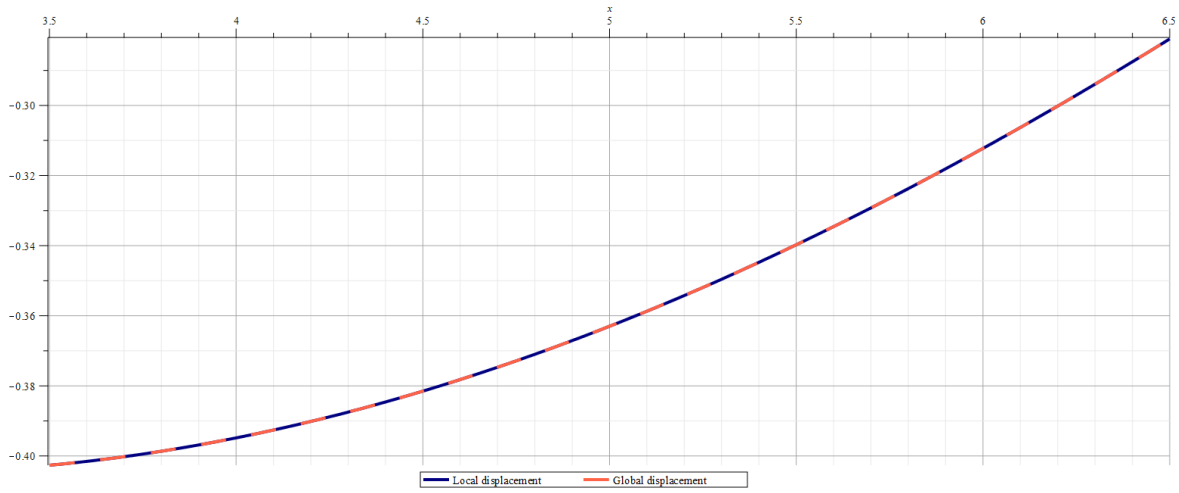

Figure 4.9: Comparison of the global and local shape of the beam at $t = 17$ s caused by the real part of excitation

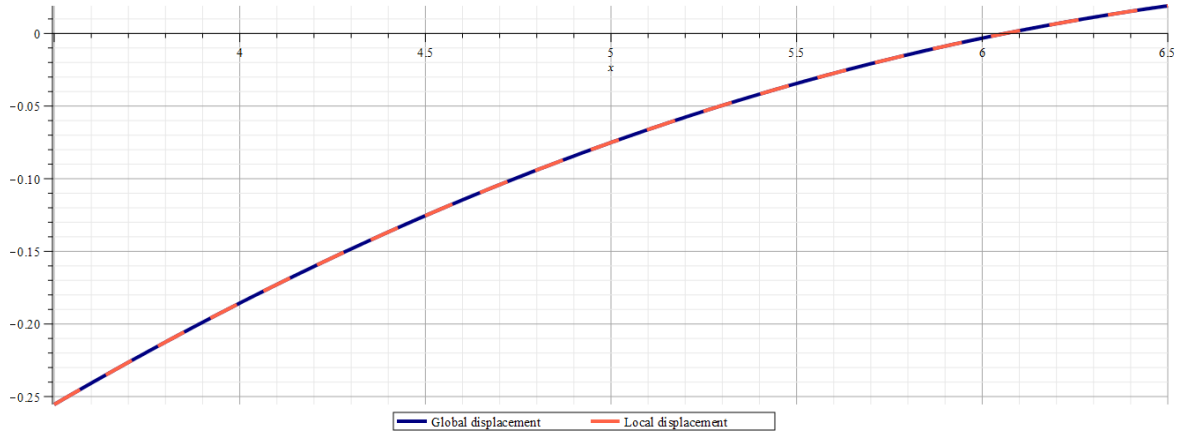

Figure 4.10: Comparison of the global and local shape of the beam at $t = 17$ s caused by the imaginary part of excitation

4.2. Step 2: Simple beam model in Flexcom

As was mentioned in the introduction, the step following the assessment of the analytical is the assessment of a simple cantilever beam problem with the use of the Flexcom software package. First the model set-up will be discussed (section 4.2.1), after which the excitation procedure is explained (section 4.2.2), followed by the results of this model(section 4.2.3) and finally the conclusion of the simple model (section 4.2.4). The goal of this assessment is to gain insight in the dynamic response in the Flexcom software and to verify that the simulation scenarios converge.

4.2.1. Model set-up

The simple beam model is constructed of a inextensible steel pipeline of 50 meters. At the top the pipe is clamped, and at the bottom it is free hanging, as can be seen in the schematic overview in figure 4.11a and the model in the Flexcom software in figure 4.11b. Both the submerged and the emerged scenarios have been studied, but since hydrodynamic damping is an important aspect, the emerged scenario has been discarded.

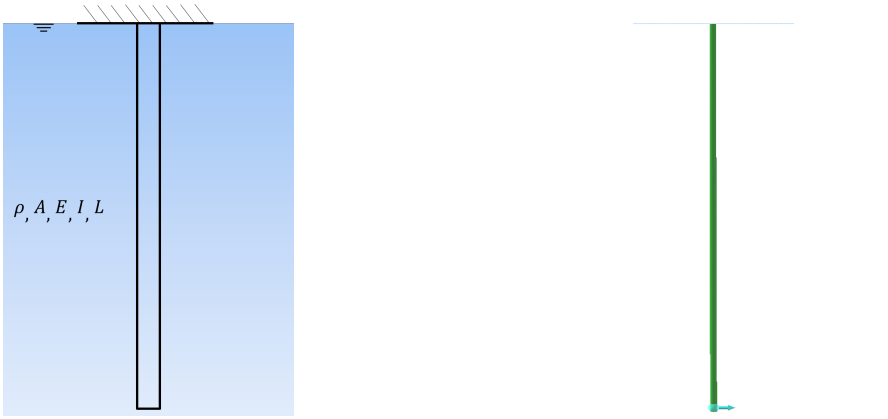

(a) Simple beam model (b) Simple beam model in Flexcom

Figure 4.11: Schematic of the simple beam model

Furthermore, the properties used for the simple model are depicted in table 4.1.

Table 4.1: Properties of simple model

Property	Value	Unit
OD	12.75	inch
WT	33.00	mm
L	50.00	m
mass per unit length	237.00	kg/m
EI	64.62	MPa
C_D	0.80	-
C_M	2.00	-

4.2.2. Excitation procedure

The DSM is calculated as the ratio between the excitation force **F** and the displacement response **u**, as was explained in section 3.2. Hence the simple model in Flexcom is excited by harmonic forces **F**. First only the harmonic axial force is applied to the system after which the displacement responses in all three DOFs are recorded. The same excitation procedure is repeated but then for the shear force and the moment. The value of the amplitude of these forces is the same for each force and is increased to study the behaviour of the simple beam. The studied amplitude values range from 1 to $1 \cdot 10^5$ for both the forces as well as the moment.

4.2.3. Results for the simple beam model

Response from Flexcom

Three selected forcing scenarios will be discussed in this subsection. One scenario with a very low force amplitude ($F = 1$N), one with a relatively moderate force amplitude ($F = 10 \cdot 10^3$N) and one with a very large force amplitude ($F = 10 \cdot 10^5$N), all with respect to the transverse static stiffness of the beam, which is: $k_{static} \approx 2kN/m$.

The displacement response for the low force amplitude scenario is shown in figure 4.12. For this scenario the first column and the top row have the response that is expected, because in a linear system an axial force does not cause a transverse displacement or rotational response and in return a tangential displacement response is not caused by a shear force or a moment. The bottom corner however, where the shear and moment interaction is plotted, does show a displacement response. Unfortunately it is a very noisy response, this is due to the hydrodynamic damping. The force and thus the velocity of the pipe is very low, in the Morison equation the velocity is squared resulting in an even smaller number, which results in small drag damping. The system does not find its steady state with this very small damping.

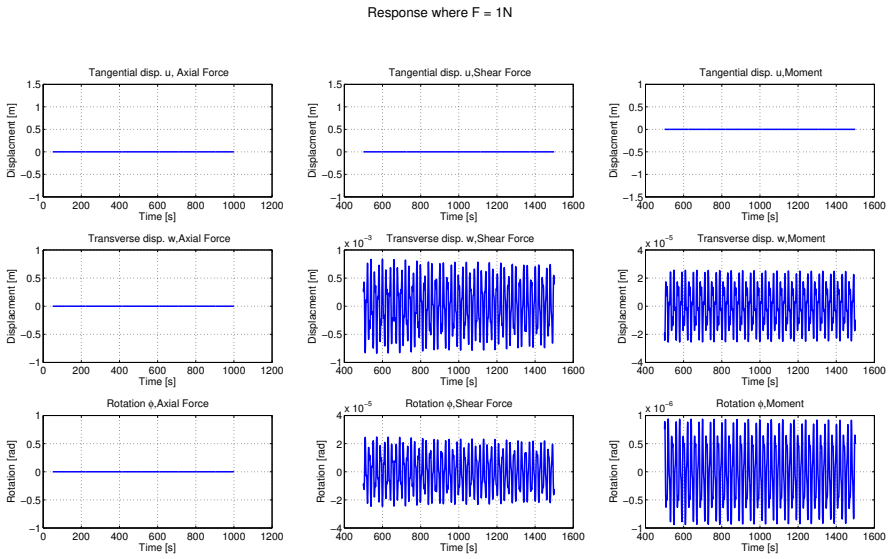

Figure 4.12: Displacement response $F_{shear} = F_{axial} = 1N$ and $M = 1Nm$

For the moderate scenario the response is shown in figure 4.13, note that in these graphs a steady state was reached and that just the last 250 seconds are shown. Again the first column gives an expected result, with the only displacement response that reacts to an axial force being the tangential. The top row however gives an unexpected response, with a tangential displacement being caused by both a shear force and a moment. These displacement responses are due to the non-linear coupling of the DOFs, in other words: due to the large axial stiffness of the short beam, it moves around an arc with the radius that has the length of the beam. The software records this movement along the arc as a tangential displacement. As for the right bottom quadrant it can be seen that the response has become more regular than for the first scenario. The response assumes a regular harmonic wave with the same period as the excitation ($T = 20$)s. Since the absolute value of the force amplitude is the same for each force DOF, the absolute value of the amplitude of the responses can be compared. This comparison between responses provides insight into the symmetric requirement of the DSM. When comparing the rotation due to a shear force and the transverse displacement due to a moment, the absolute value of the amplitudes are similar and thus the symmetric requirements are fulfilled.

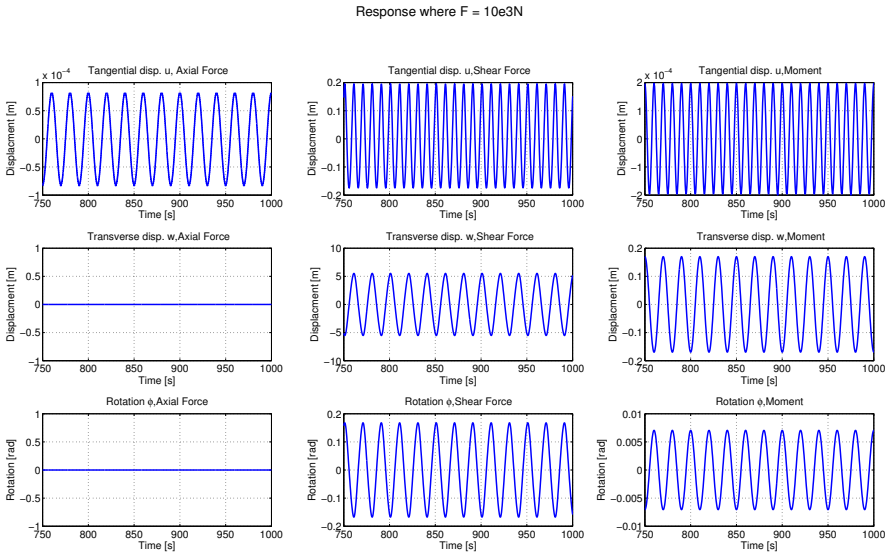

Figure 4.13: Displacement response $F_{shear} = F_{axial} = 10 \cdot 10^3 N$ and $M = 10 \cdot 10^3 Nm$

Finally the last scenario is shown in figure 4.14, again the last 250 seconds are shown in the graphs. These graphs are very similar to the ones of the moderate force amplitude in figure 4.13. Apart from the absolute value of the amplitudes there are no distinct differences between the displacement responses in itself, there is however a difference in the symmetric properties. When comparing the rotation due to a shear force and the transverse displacement due to a moment for this excitation force, the absolute value of the amplitudes are not similar and thus the symmetric requirements are not fulfilled. This implies that the system's displacement response is no longer linear.

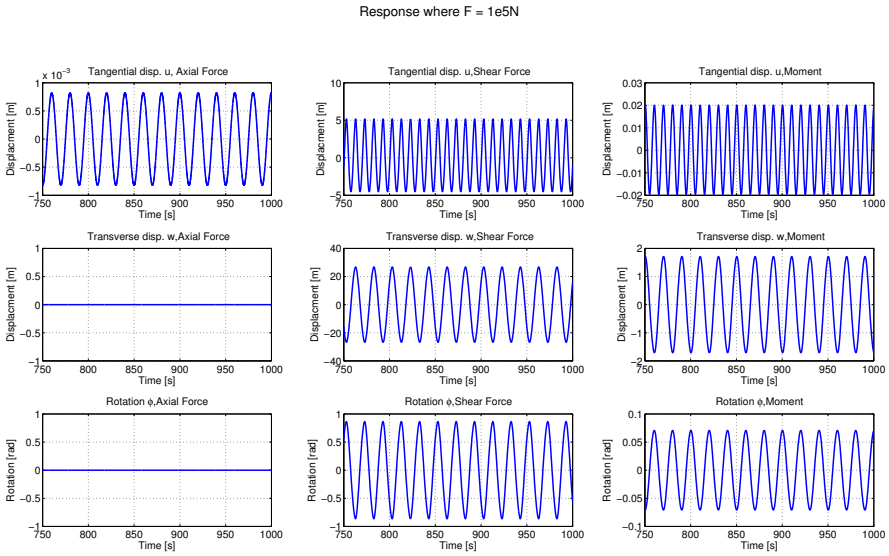

Figure 4.14: Displacement response $F_{shear} = F_{axial} = 1 \cdot 10^5 N$ and $M = 1 \cdot 10^5 Nm$

Dynamic Stiffness Matrix

From all the studied force scenarios the responses for the load amplitudes equal to $10 \cdot 10^3$ are the most linear, so this scenario is used to calculate the DSM of the simple beam model. As described in Phase 4 of section 3.2 this is done using a FFT. The result of the FFT of these displacement responses is shown in figure 4.15

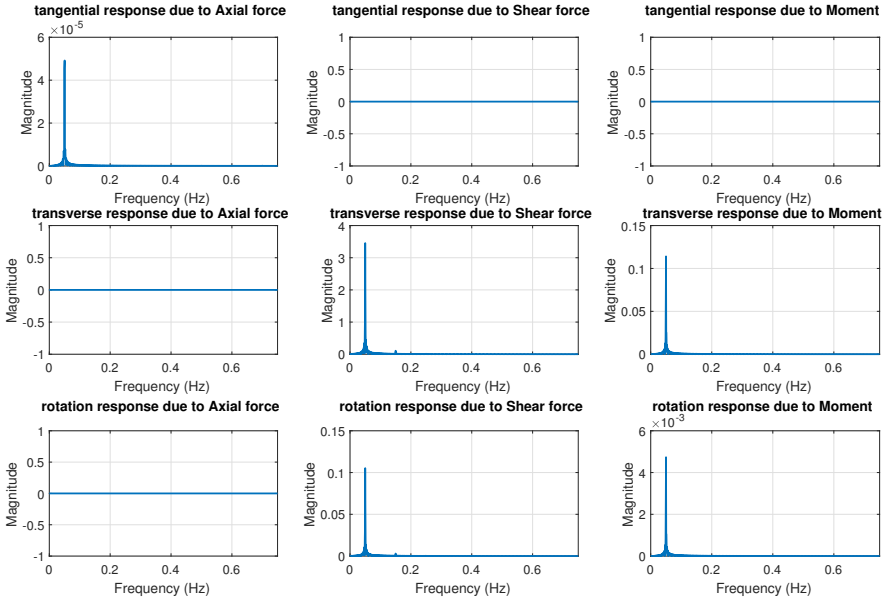

Figure 4.15: Frequency spectra of displacement response to $F_{axial} = F_{shear} = 10 \cdot 10^3$N, $M = 10 \cdot 10^3$Nm

The values for the Flexibility Matrix can be calculated from these spectra, as was explained with equation 3.3. In equation 4.19 the Flexibility Matrix is shown.

$$\textbf{Flexibility Matrix}(\Omega = \Omega_{ex}) = \begin{bmatrix} 4.91 \cdot 10^{-9} - 1.7 \cdot 10^{-25} i & 00.0 + 00.0i & 00.0 + 00.0i \\ 00.0 + 00.0i & 3.45 \cdot 10^{-4} - 1.15 \cdot 10^{-20} i & 1.14 \cdot 10^{-5} - 4.0 \cdot 10^{-22} i \\ 00.0 + 00.0i & 1.05 \cdot 10^{-5} - 3.5 \cdot 10^{-22} i & 4.73 \cdot 10^{-7} - 1.6 \cdot 10^{-24} i \end{bmatrix} \tag{4.19}$$

Thereafter the DSM in 4.20 can be calculated from the Flexibility Matrix in 4.19. By definition, the inverse of a symmetric matrix is also symmetric, thus the DSM is also symmetric as can be seen in equation 4.20.

$$\textbf{DSM}(\Omega = \Omega_{ex}) = \begin{bmatrix} 2.04 \cdot 10^{8} + 7.05 \cdot 10^{-9} i & 00.0 + 00.0i & 00.0 + 00.0i \\ 00.0 + 00.0i & 1.09 \cdot 10^{4} + 3.25 \cdot 10^{-13} i & -2.62 \cdot 10^{5} - 7.5 \cdot 10^{-12} i \\ 00.0 + 00.0i & -2.42 \cdot 10^{5} - 7.33 \cdot 10^{-12} i & 7.93 \cdot 10^{6} + 2.41 \cdot 10^{-10} i \end{bmatrix} \tag{4.20}$$

This DSM has some differences compared to the DSM of the top part of the analytical model. Besides from the extra DOF, there are two other differences that need to be mentioned. These differences apply to the right lower quadrant, which comprises the transverse and rotational DOFs. The first difference is the sign change of the non-diagonal values, for the analytical model (eq. 4.17) these were positives. The signs change because of different vertical axis convention in the Flexcom software that is why the right lower quadrant of this DSM has the same signs as the DSM of the right lower part of the analytical model (eq. 4.18), that has the same vertical axis direction. The second difference that needs to be mentioned is the small difference of the real values of the non-diagonal part, this is caused by small numerical errors in the calculation.

4.2.4. Conclusion of simple model

The most important conclusion that can be drawn from the results of the simple model is the fact that it is possible to use the Flexcom software to calculate Dynamic Stiffness Matrices. Other conclusions are:

- For small excitations the displacement responses are noisy due to hydrodynamic damping.
- Non-linear coupling between the DOFs is present.

4.3. Step 3: Pipeline model

In the previous section, it was concluded that it is possible to calculate DSMs for a simple model with the Flexcom software and thus that it should be possible to do the same for the more complex pipeline configuration. This section is dedicated to the set up of this more complex pipeline configuration and the results of this model.

4.3.1. Model set-up

In the figures 4.16a and 4.16b below, the set-up of the pipeline model is shown.

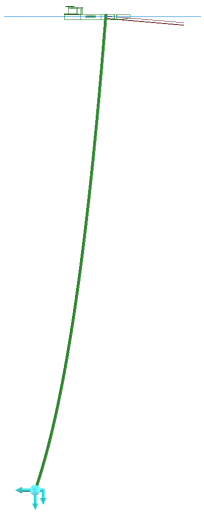

(a) Top part of the pipeline in Flexcom

(b) Bottom part of the pipeline in Flexcom

Figure 4.16: Pipeline model in Flexcom

The build-up of these models was already briefly mentioned in Phase 2 of section 3.2, but a more elaborate explanation is given below.

Top part

The reaction forces at the top cut-off are obtained from the complete global model, after which everything below the cut-off is removed from the Flexcom script, creating an almost vertical free hanging pipe. The bottom end is then loaded by the static reaction forces, bringing the pipeline to its catenary shape. At the vessel it is assumed that the pipeline is clamped, i.e constrained in all 6 DOFs.

Bottom part

The reaction forces at the lower cut-off are obtained for the bottom part, only this time everything above the cut-off is removed from the Flexcom script. The short segment remaining is loaded at the top end by the static reaction forces as was done for the top part, bringing it to its original shape. The pipeline is assumed to be hinged at the TDP, i.e. constrained in 5 DOFs, only rotation around the z-axis (figure 1b for axis configuration) is allowed. Furthermore, the interaction with the soil is assumed to be infinitely stiff.

4.3.2. Excitation procedure

The procedure of excitation is basically the same as with the simple model. A harmonic load is applied separately for the axial force and the shear force and the bending moment. The difference however with the simple model is that the pipe segments are not perfectly vertical. Due to the catenary shape of the

whole pipeline, the remaining parts of the pipeline are under an angle. In theory this is not a problem for a force excitation. Instead of forcing in the global axis system, the forcing takes place in the local axis system. Unfortunately the Flexcom software only computes force input in the global axis, therefore the local harmonic forces needed to be transferred from the local to the global axis system. Furthermore, the magnitude of force amplitudes is different for each force DOF. For the pipeline model each force DOF is loaded by a percentage of its corresponding static force. In equation 4.21 an example of this is shown, demonstrating the harmonic force in the local axial direction where the amplitude of this harmonic is chosen with a certain percentage, α%, of the static force in the local axial direction.

$$\mathbf{F_{Harmonic,Axial}} = \begin{bmatrix} \hat{F}_{Static,Axial} & + & \alpha\% \cdot \hat{F}_{Static,Axial} \cdot \cos(\Omega t) \\ \hat{F}_{Static,Shear} & + & 0\% \cdot \hat{F}_{Static,Shear} \cdot \cos(\Omega t) \\ \hat{F}_{Static,Moment} & + & 0\% \cdot \hat{F}_{Static,Moment} \cdot \cos(\Omega t) \end{bmatrix} \tag{4.21}$$

Here again it is assumed that small perturbations are linear. The only difference with the simple model is that these small perturbations are around the Geometric Non-Linear equilibrium. Because of this assumption, small percentages of the static forces are used in order to remain in the linear domain.

5

Results of the enhanced methodology

5.1. Response of the pipeline model

For the pipeline model not one, but two sets of displacement responses are recorded. One set for the top part and one for the bottom part. In principle these displacement responses look the same as those of the simple model. In figures 5.1a and 5.1b both the top and the bottom displacement responses are shown. With along the vertical axis the response and the horizontal axis the time. The harmonic force amplitude for both is 1% of the corresponding static forces, but looking at the graphs it becomes immediately clear that the responses are significantly different. Therefore, the responses of the top part and the bottom part are discussed separately.

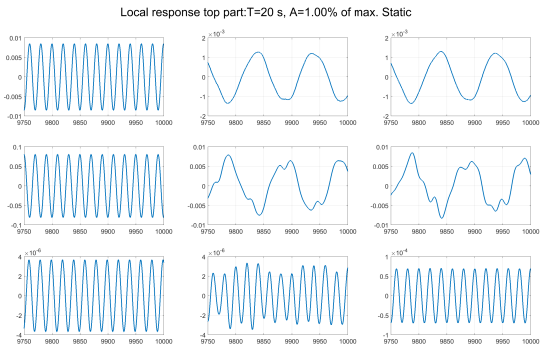

(a) Displacement response of the top part

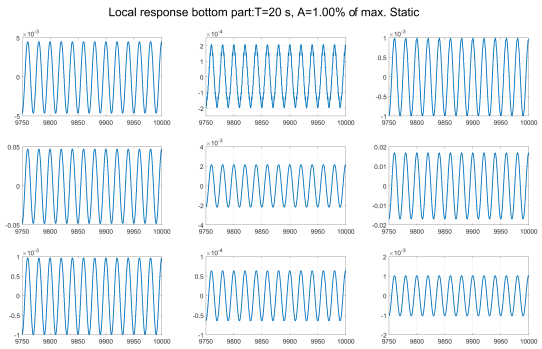

(b) Displacement response of the bottom part

Figure 5.1: Displacement responses

5.1.1. Top part

As was explained in section 4.3.2, the total load or moment acting on the pipeline is composed of a static reaction force and a dynamic amplitude that is a percentage of the static force, these percentages are shown in appendix A. At 1% of the static forces the displacement responses of the top part are very irregular. Only the axial excitation displayed in the first column converges to a steady state response. The cause of this is found in the magnitude of the static forces, displayed in table 5.1.

Table 5.1: Static reaction forces top part

Force DOF	Value	Unit
Axial	$586.25 \cdot 10^3$	N
Shear	$0.17 \cdot 10^3$	N
Moment	$43.07 \cdot 10^3$	Nm

The top part of the model is in a near vertical position resulting in a large axial force and a low shear force, the static shear force is ~ 0.03% of the static axial force. The value of the shear force needs to be very large in order to have an influence on the top part, where a small value of the axial force is sufficient to generate a regular response. The large difference of influence that the forces have on the model demands that each force DOF is examined separately.

Axial force

The axial force is dominant in the model of the top part. This results in a regular response for small amplitude values. A regular response for the axial force is at ~ 5% of the static axial force (~ 615 kN).

Shear force

Due to the small influence of the shear force on the model of the top part, large amplitudes are required to have significant displacement response. The displacement responses for the shear force start to converge to a steady state at ~ 100% of the static shear force (~ 340 N).

Moment

The influence of the moment on the model of the top part is also small compared to the axial force. Large amplitudes are therefore required to result in a significant displacement response. The displacement responses for the moment start to converge to a steady state at ~ 125% of the static moment (~ 97 kNm).

5.1.2. Bottom part

The displacement responses of the bottom part display a regular harmonic response with the period equal to the period of the excitation. This regular response is because of three reasons, firstly the static reaction forces (table 5.2) which have a relatively smaller difference to each other compared to the top part (table 5.1), secondly the orientation of the pipeline is almost horizontal, and lastly the length of the pipe segment near the seabed is much shorter, with the bottom part being almost 74 meters compared to more than 1,500 meters of the top part.

Table 5.2: Static reaction forces bottom part

Force DOF	Value	Unit
Axial	$190.94 \cdot 10^3$	N
Shear	$1.36 \cdot 10^3$	N
Moment	$360.49 \cdot 10^3$	Nm

Due to the more regular response of the bottom part it is not necessary to discuss each force DOF separately in this section.

5.1.3. Dynamic Stiffness Matrix

The dynamic stiffness matrix is described as $\mathbf{Z}(\omega) = -\omega^2\mathbf{M} + i\omega\mathbf{C} + \mathbf{K}$, as was shown in section 2.4.2. From this equations a real part: $\mathbf{K} - \omega^2\mathbf{M}$, and an imaginary part: $\omega\mathbf{C}$, can be separated. In order to determine the values of the DSM, one could use a simple mass, spring and dash-pot system to determine the expressions of the aforementioned real and imaginary parts. The system shown below in figure 5.2 is used to determine these expressions.

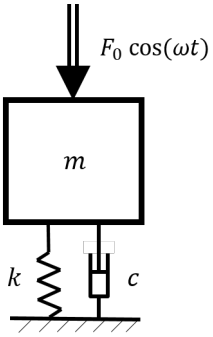

Figure 5.2: Mass with a spring dash-pot system

With the equation of the system being equation 5.1 and the general solution being 5.2:

$$m\ddot{x} + c\dot{x} + kx = F_0\cos(\omega t) \tag{5.1}$$
$$x = x_0\cos(\omega t + \phi) \tag{5.2}$$

Where in this case x_0 is the amplitude of the response and ϕ is the phase shift.
Inserting the solution into the equation results into the expression shown in equation 5.3.

$$(-c\omega x_0\sin(\phi) - (\omega^2 m - k)x_0\cos(\phi))\cos(\omega t) + (-c\omega x_0\cos(\phi) + (\omega^2 m - k)x_0\sin(\phi))\sin(\omega t) = F_0\cos(\omega t) \tag{5.3}$$

Separating the terms in equation 5.3 with respect to $cos(\omega t)$ and $sin(\omega t)$, results in two equations that have to equal to zero, see equations 5.4 and 5.5:

$$-c\omega x_0\cos(\phi) + (\omega^2 m - k)x_0\sin(\phi) = 0 \tag{5.4}$$
$$-c\omega x_0\sin(\phi) - (\omega^2 m - k)x_0\cos(\phi) - F_0 = 0 \tag{5.5}$$

Then the expression for the real and imaginary part of the DSM is calculated with the equations 5.4 and 5.5, resulting in equations 5.6 and 5.7.

$$k - \omega^2 m = \frac{F_0}{x_0}\cos(\phi) \tag{5.6}$$
$$\omega c = -\frac{F_0}{x_0}\sin(\phi) \tag{5.7}$$

These expressions hold for a 1DOF system, but the pipeline is a 3DOF system. Moreover the pipeline is excited by a force and therefore the DSM can not be directly obtained from the amplitudes and phase shift. First the compliance matrix **Y**, which is the inverse of the DSM must be calculated. This is done with equations 5.8 and 5.9, where k is the displacement DOF, j the force DOF and m and n are the matrix indices.

$$Re(\mathbf{Y}_{m,n}) = \frac{x_k}{F_j}\cos(\phi) \tag{5.8}$$
$$Im(\mathbf{Y}_{m,n}) = -\frac{x_k}{F_j}\sin(\phi) \tag{5.9}$$

Since the amplitude of the force on the pipeline is known beforehand, and the amplitude and phase shift of the response of the pipeline can be calculated from the results of the Flexcom analyses, this approach is applicable to this model. Therefore, these expressions are used to calculate the compliance matrices of the top and bottom part of the pipeline. This is done for the compliance matrix per force DOF separately as is shown in the matrix 5.10. Taking the inverse results in the desired DSMs

$$\mathbf{DSM}^{-1} = \mathbf{Y} =$$
$$\begin{bmatrix} \left(\frac{x_u}{F_a}\cos(\phi_{u,F_a})\right)+\left(-\frac{x_u}{F_a}\sin(\phi_{u,F_a})\right)i & \left(\frac{x_w}{F_a}\cos(\phi_{w,F_a})\right)+\left(-\frac{x_w}{F_a}\sin(\phi_{w,F_a})\right)i & \left(\frac{x_\theta}{F_a}\cos(\phi_{\theta,F_a})\right)+\left(-\frac{x_\theta}{F_a}\sin(\phi_{\theta,F_a})\right)i \\ \left(\frac{x_u}{F_s}\cos(\phi_{u,F_s})\right)+\left(-\frac{x_u}{F_s}\sin(\phi_{u,F_s})\right)i & \left(\frac{x_w}{F_s}\cos(\phi_{w,F_s})\right)+\left(-\frac{x_w}{F_s}\sin(\phi_{w,F_s})\right)i & \left(\frac{x_\theta}{F_s}\cos(\phi_{\theta,F_s})\right)+\left(-\frac{x_\theta}{F_s}\sin(\phi_{\theta,F_s})\right)i \\ \left(\frac{x_u}{M}\cos(\phi_{u,M})\right)+\left(-\frac{x_u}{M}\sin(\phi_{u,M})\right)i & \left(\frac{x_w}{M}\cos(\phi_{w,M})\right)+\left(-\frac{x_w}{M}\sin(\phi_{w,M})\right)i & \left(\frac{x_\theta}{M}\cos(\phi_{\theta,M})\right)+\left(-\frac{x_\theta}{M}\sin(\phi_{\theta,M})\right)i \end{bmatrix} \tag{5.10}$$

Where:

- F_a :The axial force excitation [N]
- F_s : The shear force excitation [N]
- M : The moment excitation [Nm]
- x_u : The displacement in the tangential(=axial) direction [m]
- x_w : The displacement in the transverse(=shear) direction [m]
- x_θ : The in-plane rotational displacement [rad]
- $\phi_{k,j}$: The phase shift of the response k to the force excitation j [rad]

Top part

The DSM of the top part is calculated with the matrix shown in equation 5.10. In order to do this the force amplitude, the response amplitudes and the phase shifts are required. In the following plots shown in figures 5.3 to 5.5, these amplitudes and phase shift are shown per force DOF excitation, first the axial force, then the shear force and finally the moment excitation. The $\phi_{k,j}$ is determined with a zero-down crossing method.

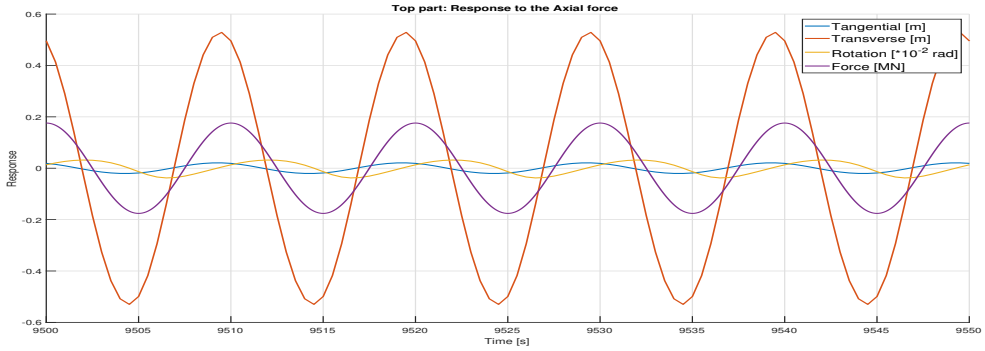

Figure 5.3: Response of the top part caused by the Axial force

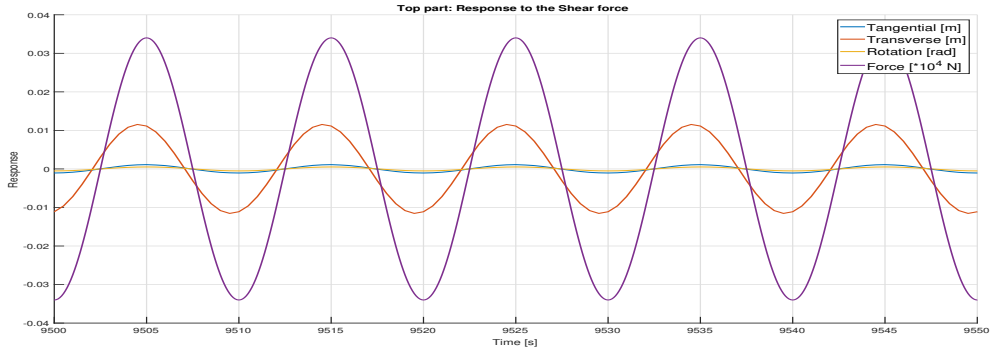

Figure 5.4: Response of the top part caused by the Shear force

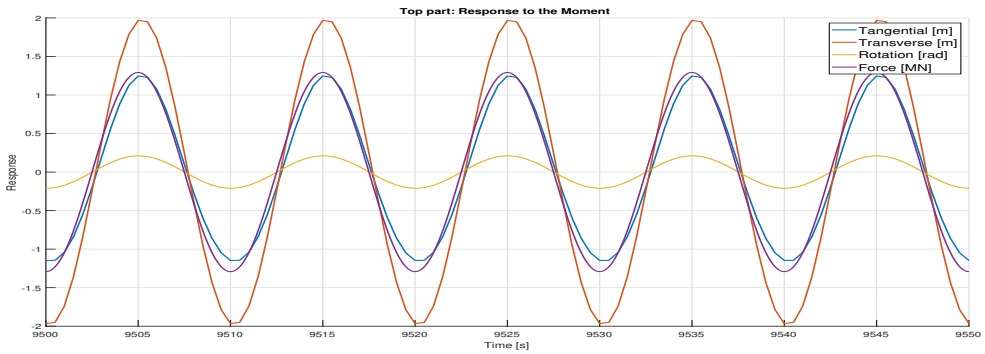

Figure 5.5: Response of the top part caused by the Moment

Using the values from the figures and equation 5.10, the compliance matrix of the top part becomes:

$$\mathbf{Y}(\Omega=\Omega_{ex}) = \begin{bmatrix} 9.99\cdot10^{-8}+6.34\cdot10^{-8}i & 3.11\cdot10^{-6}+9.84\cdot10^{-7}i & 9.64\cdot10^{-7}+0.00i \\ 2.54\cdot10^{-6}+1.61\cdot10^{-6}i & 3.22\cdot10^{-5}+1.07\cdot10^{-5}i & 1.52\cdot10^{-6}+0.00i \\ 4.50\cdot10^{-10}+1.75\cdot10^{-9}i & 1.51\cdot10^{-6}+0.00i & 1.64\cdot10^{-7}+0.00i \end{bmatrix} \tag{5.11}$$

$$\mathbf{DSM}(\Omega=\Omega_{ex}) = \begin{bmatrix} -2.74\cdot10^{6}+7.41\cdot10^{5}i & 3.89\cdot10^{5}-2.07\cdot10^{5}i & -3.61\cdot10^{6}+1.93\cdot10^{6}i \\ 3.95\cdot10^{5}-9.29\cdot10^{4}i & -1.55\cdot10^{4}+3.66\cdot10^{3}i & 1.44\cdot10^{5}-3.39\cdot10^{4}i \\ -3.65\cdot10^{6}+8.58\cdot10^{5}i & 1.44\cdot10^{5}-3.38\cdot10^{4}i & 4.77\cdot10^{6}+3.14\cdot10^{5}i \end{bmatrix} \tag{5.12}$$

There are multiple things about this DSM that have to be mentioned:

- There are negative terms on the diagonal, this is not as expected, but it is possible when the system is inertia dominated, i.e. $\omega^2 m > k$.
- It is not symmetric for the coupling between the axial DOF and the rotational DOF(bottom left and upper right in the matrix). This is also not as expected and could be due to non-linear coupling of DOFs.
- The signs of the lower quadrant are different then expected compared to the simple beam model.
- The right lower quadrant is however symmetric.
- The errors in this matrix could explain the errors in the Flexcom analysis.
- The response of the axial displacement on the moment and the rotation to the axial force were small, maybe these could neglected, resulting in a much more symmetric matrix.

Bottom part

The same procedure is repeated for the bottom part. The values for the amplitude and phase shift are plotted in the figures 5.6 to 5.8.

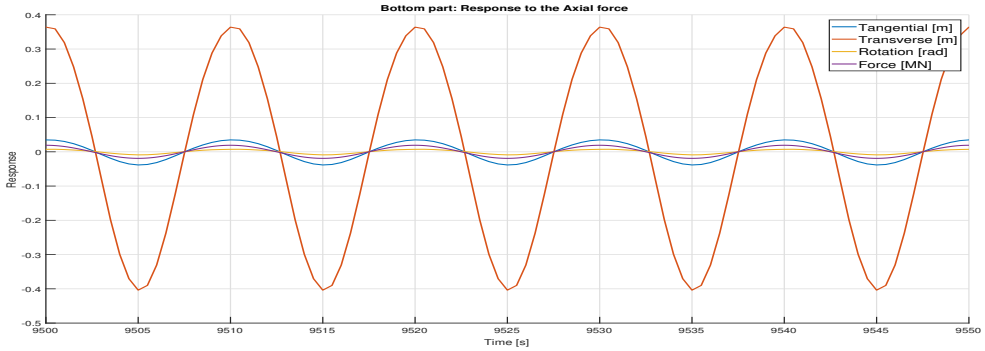

Figure 5.6: Response of the bottom part caused by the Axial force

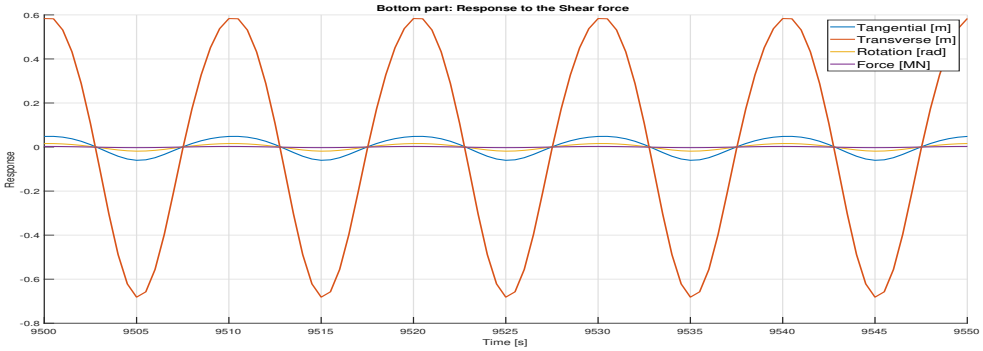

Figure 5.7: Response of the bottom part caused by the Shear force

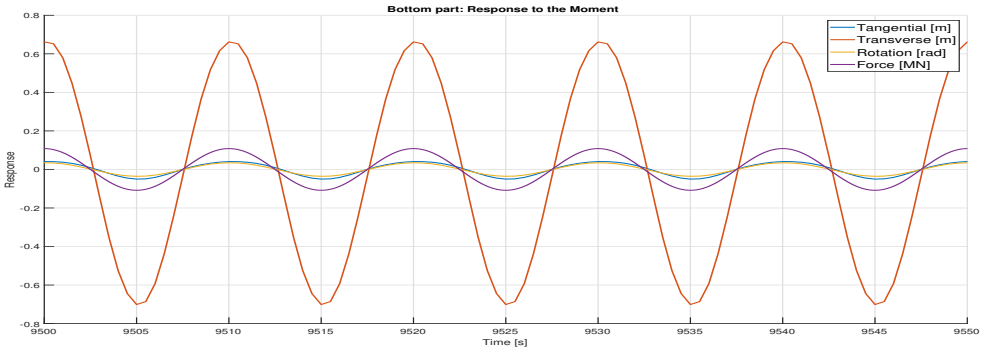

Figure 5.8: Response of the bottom part caused by the Moment

For the bottom part of the pipeline, using the values from the graphs, the **Y** then becomes:

$$\mathbf{Y}(\Omega = \Omega_{ex}) = \begin{bmatrix} 1.82 \cdot 10^{-6} - 1.14 \cdot 10^{-7} i & 1.77 \cdot 10^{-5} - 1.11 \cdot 10^{-6} i & 3.76 \cdot 10^{-7} - 2.36 \cdot 10^{-8} i \\ 1.9 \cdot 10^{-5} - 1.19 \cdot 10^{-6} i & 2.14 \cdot 10^{-4} - 1.35 \cdot 10^{-5} i & 6.10 \cdot 10^{-6} - 3.84 \cdot 10^{-7} i \\ 3.85 \cdot 10^{-7} - 2.42 \cdot 10^{-8} i & 5.82 \cdot 10^{-6} - 3.66 \cdot 10^{-7} i & 3.17 \cdot 10^{-7} - 3.17 \cdot 10^{-8} i \end{bmatrix} \tag{5.13}$$

Inverting the compliance matrix gives the DSM:

$$\mathbf{DSM}(\Omega = \Omega_{ex}) = \begin{bmatrix} 7.89 \cdot 10^{6} + 4.96 \cdot 10^{5} i & -8.39 \cdot 10^{5} - 5.28 \cdot 10^{4} i & 6.81 \cdot 10^{6} + 4.28 \cdot 10^{5} i \\ -8.98 \cdot 10^{5} - 5.65 \cdot 10^{4} i & 1.05 \cdot 10^{5} + 6.62 \cdot 10^{3} i & -9.62 \cdot 10^{5} - 6.05 \cdot 10^{4} i \\ 6.87 \cdot 10^{6} + 4.32 \cdot 10^{5} i & -9.10 \cdot 10^{5} - 5.73 \cdot 10^{4} i & 1.25 \cdot 10^{7} + 7.87 \cdot 10^{5} i \end{bmatrix} \tag{5.14}$$

Comparing this DSM to the analytical model, the signs are equal to the lower DSM of the analytical model. Regarding the symmetry of this DSM, the values are approximately equal and the small differences are most likely caused by numerical errors. The DSM for the bottom part can be implemented into the subroutine. How this is done is explained in section 5.3.2.

5.1.4. Conclusion of the pipeline model

From the calculations of the pipeline model it can be concluded that, though it is more complex, it is possible to calculate the DSMs. Furthermore it is interesting that each force DOF has a different range of amplitude values for which the response is a regular, linear response. Since the frequency based dynamic substructuring method is only applicable for linear systems. Further research was performed to find the linear domain for the top and bottom part for each displacement DOF, the results of this are shown in section 5.2.

5.2. Linear domain analysis

In this section the amplitudes of the responses are compared with the excitation amplitudes, all the used amplitudes are shown tables A.1 and A.2 in the appendix A. From the first analyses of the top part, shown on the left in figure 5.9, the small influence of the shear force and moment on the top part is confirmed. Therefore the percentages for these amplitude values needed to be increased. From right column of figure 5.9 it becomes clear that for small amplitude values all displacement responses of the bottom part respond linear. Because of the difference in displacement responses the linear analyses for bottom and top part are discussed separately. The top part is discussed in 5.2.1 and the linear analysis of the bottom part in 5.2.2. Both analyses were performed with 2 different excitation periods; $T = 20$ seconds and $T = 10$ seconds, where $T = 20$ s is the base case and $T = 10$ s is chosen because it is the critical period of this pipeline configuration.

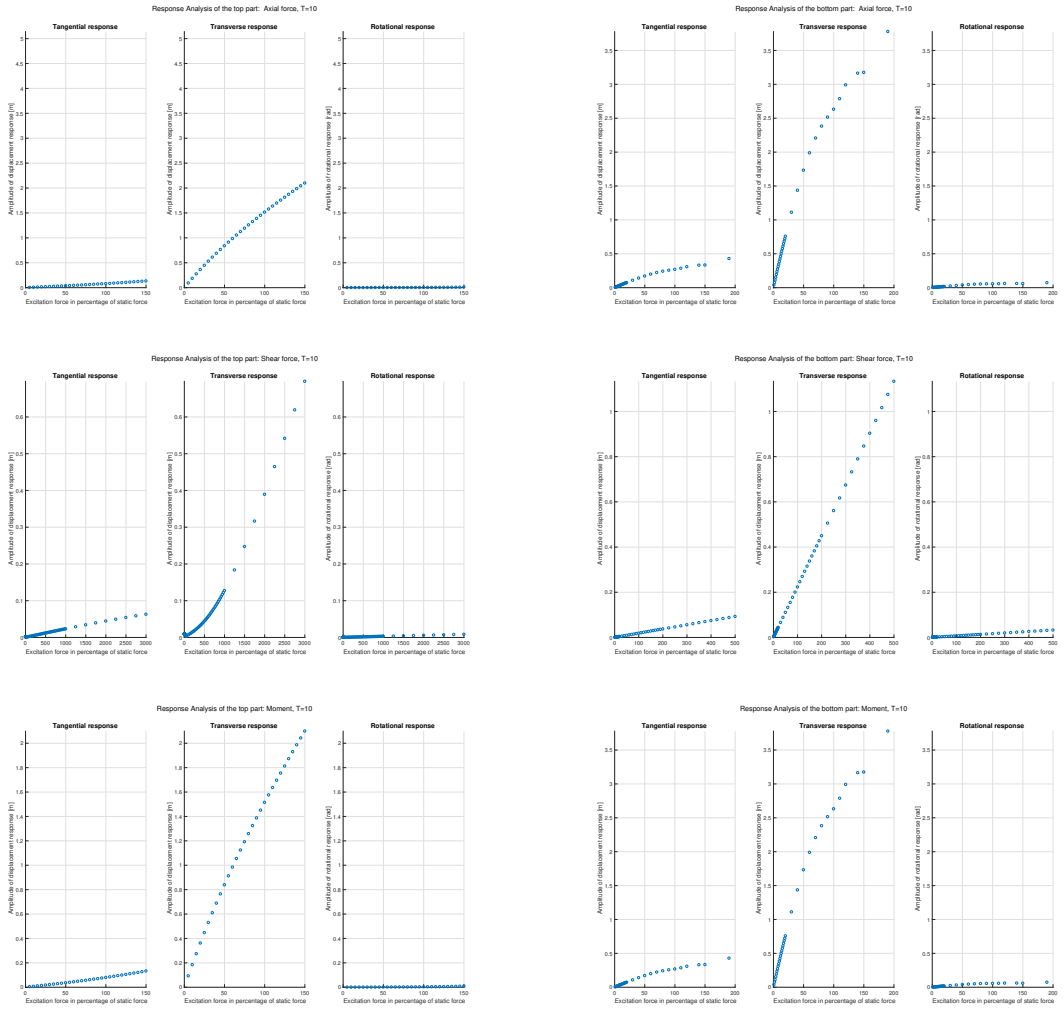

Figure 5.9: Overview of the linear analysis. Left = Top part and Right = Bottom part

In the following subsections the responses are shown per force DOF. For each force DOF a figure containing 3 graphs is shown. The graph on the left is the tangential response, the middle graph the transverse and the right graph is the rotational response. The graphs are discussed from left to right in each subsection. Moreover a red line is drawn in these graphs, this red line is the maximum measured load of a critical sea state scenario. The properties of the critical sea state for this pipeline configuration are; $H_s = 3$m and $T_p = 10$s.

5.2.1. Top part

Axial

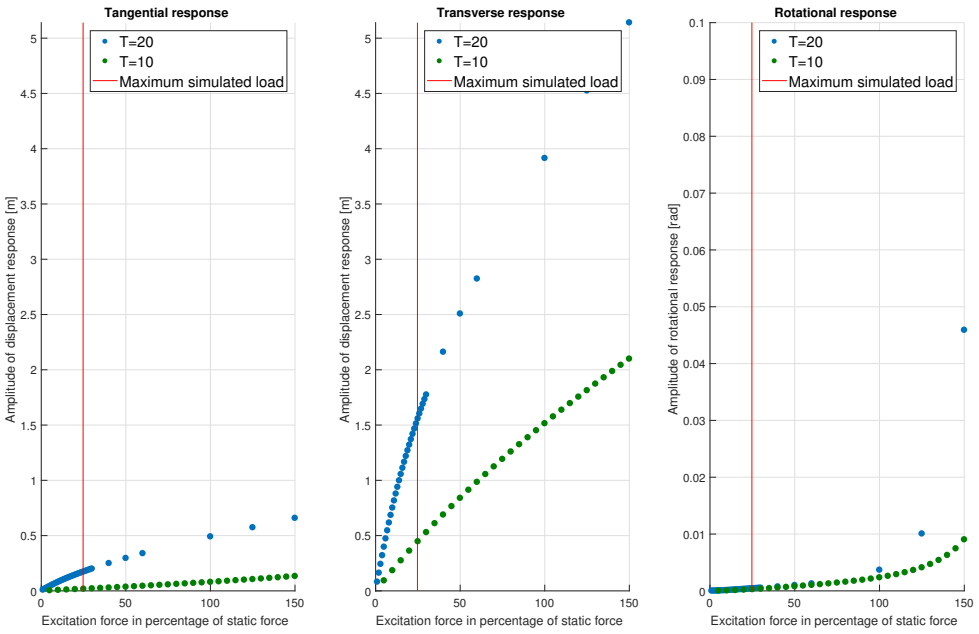

Figure 5.10: Linear Analysis top part: Excited by Axial force **NB:** Vertical axis of the right figure is 50x smaller

Left This is the tangential response caused by the axial excitation. For both of the periods the the response is fairly linear. The response for $T = 20$ s is larger than that of $T = 10$ s.

Middle This graph shows the transverse response to the axial excitation. This response is large due to the large horizontal component of the axial force that is larger than the shear force. This response show small non-linear behaviour for larger force amplitudes.

Right The influence of the axial force on the rotation of the top part is negligible as can be seen in the right graph of figure 5.10. The vertical axis is 50 times smaller, and still the response is very small.

Shear

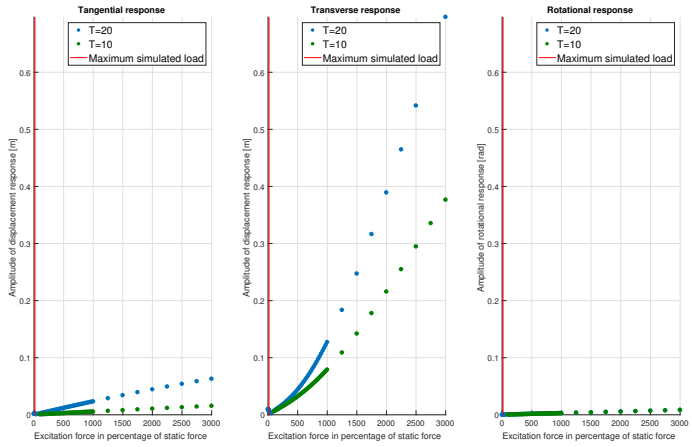

Figure 5.11: Linear Analysis top part: Excited by Shear force

Left This is the tangential response caused by the shear excitation. For both of the frequencies this response is linear up to 30 times of the static shear force (~ 5 kN).

Middle The graph in the middle displays the transverse response to the shear force. Up to ~750% of the static shear force the the excitation force is to low to influence the system. For excitation amplitudes larger than that the response is linear up to 30 times of the static shear force. Also for the shear force the response amplitude for $T = 20$ s is larger.

Right The rotational response to the shear force is displayed in the graph on the right. For both periods this response is linear and relatively small with no distinct difference between the magnitude.

Since the forcing percentage for the linear analysis is so large that the maximum simulated shear force is too close to the vertical axis. Therefore in figure 5.12 shows a zoom of figure 5.11.

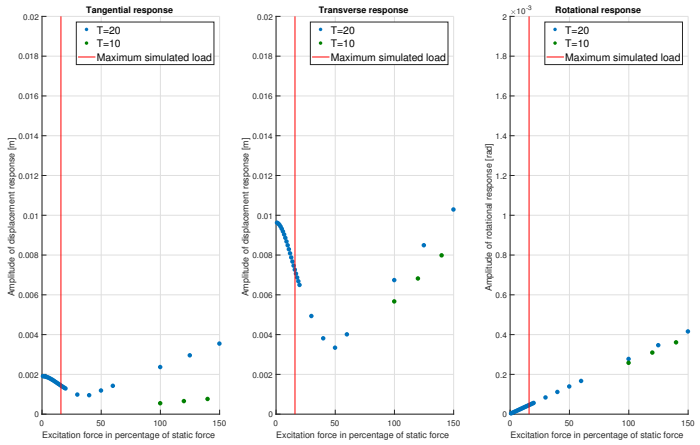

Figure 5.12: Zoom on the Linear Analysis top part: Excited by Shear force **NB:** Vertical axis of the right figure is 10x smaller

In the two most left plots of figure 5.12, a decrease in the amplitude can be seen. This decrease is caused by a non-linear second harmonic that is present for these responses, the amplitude of these non-linear second harmonics is higher than the amplitude of the linear responses. When the excitation amplitude increases, the on-linear second harmonics are damped.

Moment

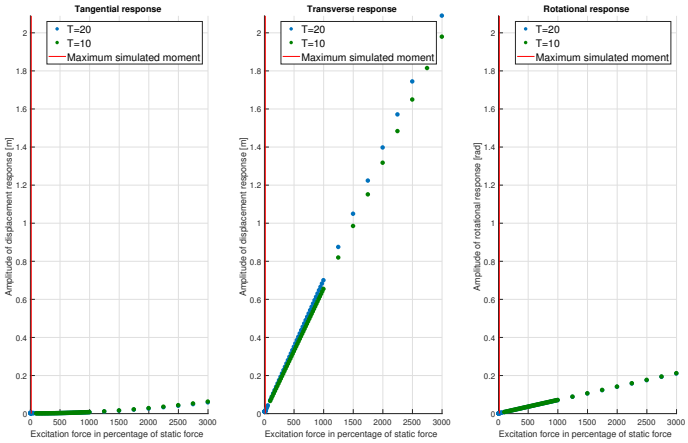

Figure 5.13: Linear Analysis top part: Excited by Moment

For all of the three graphs in figure 5.13 the difference between the response for $T = 20$ s and $T = 10$ s is very small, so The period has small influence on the displacement response of the top part caused by the moment. Furthermore all three response show linear behaviour up to 30 times of the static moment (~ 1.335 MNm).

Left The moment, as expected, has a small influence on the tangential displacement of the top part.

Middle There is a small difference between the periods, but this is negligible. It is interesting that the transverse response on the moment is larger than the rotational response to the moment.

Right The rotational responses are linear and equal for both periods.

Since the forcing percentage for the linear analysis is so large that the maximum simulated moment is too close to the vertical axis. Therefore in figure 5.14 shows a zoom of figure 5.13. The response of the tangential displacement is not affected by small amplitude moment excitation. The transverse response however is affected, but only for amplitudes above 20% $\approx$ 8.61 kNm.

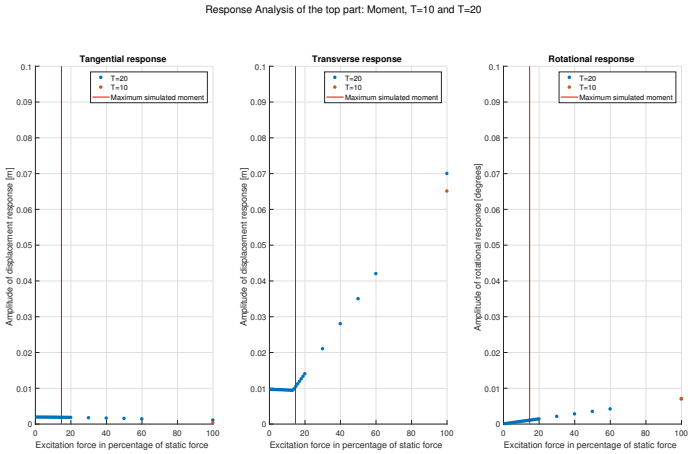

Figure 5.14: Zoom on the Linear Analysis top part: Excited by Moment

5.2.2. Bottom part

An important influence on the response of the bottom part is the influence of the seabed. For larger amplitudes of the axial force and the moment (≥ 100% of static loads) the pipe segment interacts with the seabed which is modelled as completely stiff.

Axial

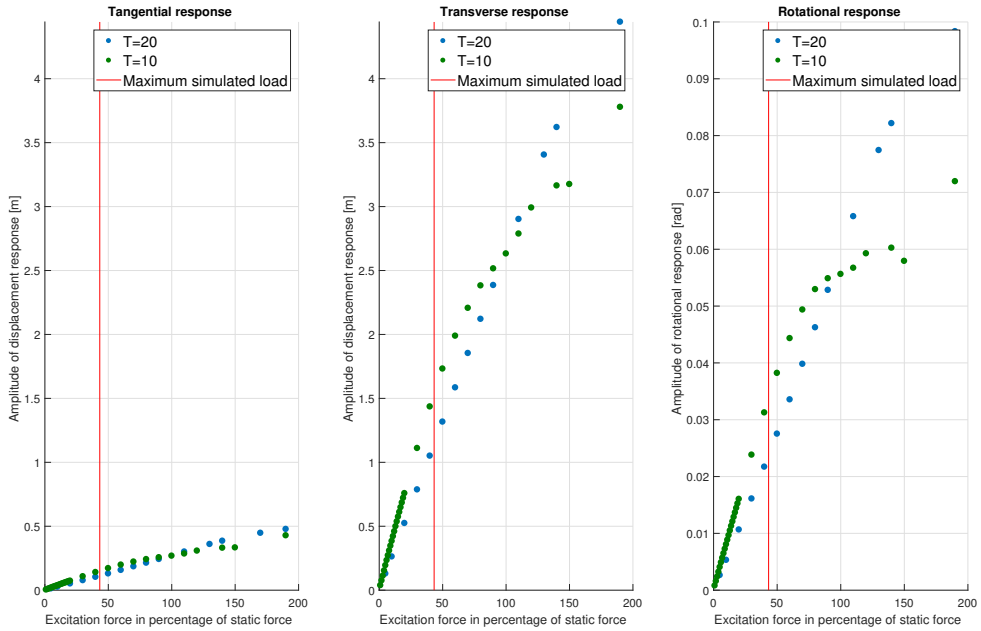

Figure 5.15: Linear Analysis bottom part: Excited by Axial force **NB:** Vertical axis of the right figure is 50x smaller

Left The responses are almost equal and fairly linear up to ~ 100% ≈ 380 kN where the pipeline interacts with the seabed. This interaction also explains the unusual jump in the response at 140%

Middle The transverse response caused by the axial force is linear for small amplitudes and non-linear starting from an amplitude larger than 100% due to seabed interaction.

Right As expected the axial force has almost no influence on the rotational response of the bottom part.

Shear

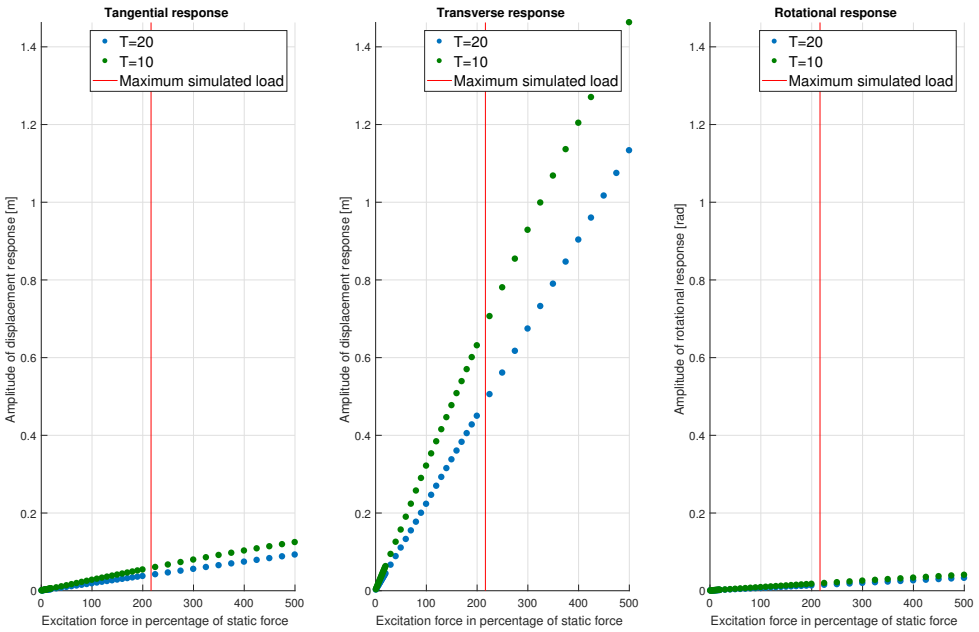

Figure 5.16: Linear Analysis bottom part: Excited by Shear force

The all three responses to the shear force are linear as figure 5.16 shows.

Left The response in the tangential direction to the shear force is small. Both periods almost overlap, though the response to the excitation with $T = 10$ s is slightly larger.

Middle In the transverse direction the response to the shear force is linear for both periods. Here again the response to the excitation with $T = 10$ s is larger.

Right The rotational response to the shear force is the smallest of the 3 displacement DOFs. There is no difference in response between the different excitation periods.

Moment

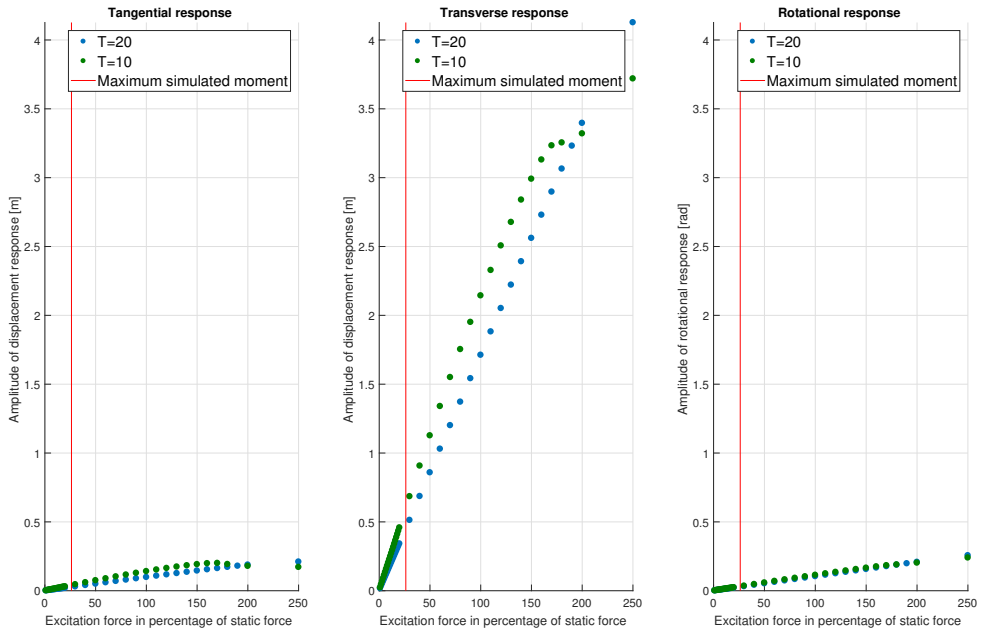

Figure 5.17: Linear Analysis bottom part: Excited by Moment

Left Similar to the axial force excitation the response is linear for small amplitudes up to ~ 100% ≈ 720 kNm where seabed interaction starts to occur.

Middle As was the case for the tangential response, the transverse response is linear for small amplitudes up to ~ 100% ≈ 720 kNm where seabed interaction starts to occur.

Right Again the rotation response is perfectly linear and equal for both excitation periods.

5.2.3. Conclusion Linear domain analysis

The most important conclusion that can be drawn from this linear domain analysis, is that the critical sea state scenario is within the linear domain of almost all the DOFs. The only exceptions are the shear force and the moment of the top part. The maximum shear force and the maximum moment measured from the critical sea state scenario are still very small and have no influence on the pipe and are below the linear domain of the shear force and moment. Therefore, a clear range of linearity needs to be determined of all the load DOF combined, this linear range is the domain where the DSM method is applicable.
Meanwhile the top part has a larger response to the excitation with $T = 20$ s, whereas the bottom part the response is larger for the excitation with $T = 10$ s, this is due to the natural periods of the parts. The natural period of the bottom part is $T \approx 6$ s and for the top part $T \approx 23$ s. The difference between the responses of the bottom part is however small compared to the difference between the responses of the top part. Furthermore, none of the rotational responses are influenced by the period, they overlap perfectly for both periods.
The rotational responses are very small for the axial and shear forces at both the top as well as the bottom part, and the influence of the moment excitation on the axial displacement is, as expected, negligible for the top part.

5.3. Demonstration Enhanced Methodology

To proof that the enhanced methodology is a viable method for dynamic FEM assessment of the sagbend, a demonstration assessment was performed. This demonstration assessment was done with the use of the Flexcom software instead of the Abaqus software which was initially proposed in the enhanced methodology. This was done due to the time constraints of the research. The approach and results are shown in sections 5.3.1 to 5.3.3.

5.3.1. FEM models for the demonstration

The main challenge when determining whether the enhanced methodology is applicable, is proving that the DSMs are correct. This proof is done stepwise in order to have more insight in the simulation. First, by testing the lower DSM that is connected through the pipeline to the vessel, then the upper DSM that is connected to the seabed and finally the combination of only the sagbend with both DSMs.
For all of the models, the following sea state was used to excite vessel motions:

Table 5.3: Properties of wave spectrum

Property	Value	Unit
Wave direction	90	degrees
H_s	3	m
T_p	10	s

Model I: Vessel to lower DSM

The first model consists of the lower DSM connected to the vessel which is excited by a single frequency harmonic wave, shown in figure 5.18. To prove whether the lower DSM is correct, the response of the pipeline for this model must be equal to that of the global model.

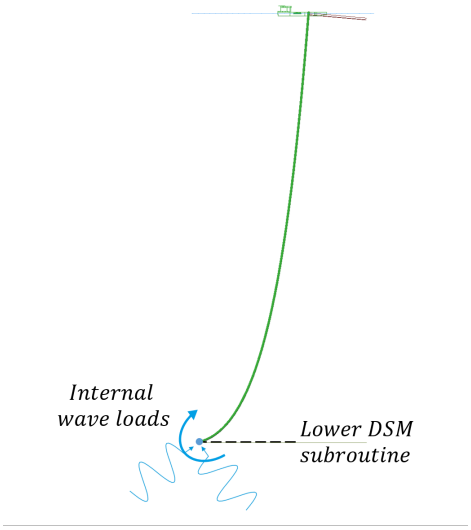

Figure 5.18: Overview of model I in Flexcom

The subroutine of this model has been constructed in two different ways. The first is a subroutine with only the stiffness(i.e. real) part of the DSM and no connection forces. The second subroutine is constructed with both the stiffness as well as the damping (i.e. real and imaginary) parts of the DSM. The connection force were also implemented in this subroutine, these connection forces are displayed in appendix B. The results of both approaches are shown in the next section.

Results of Model I

The results of the first subroutine approach are shown in the graphs in figure 5.19. It becomes clear that only the transverse response is approximately equal to the global transverse response. The other response are approaching the global response, but significant errors are still present in that response. It needs to be investigated if these errors occur from model errors or from numerical errors.

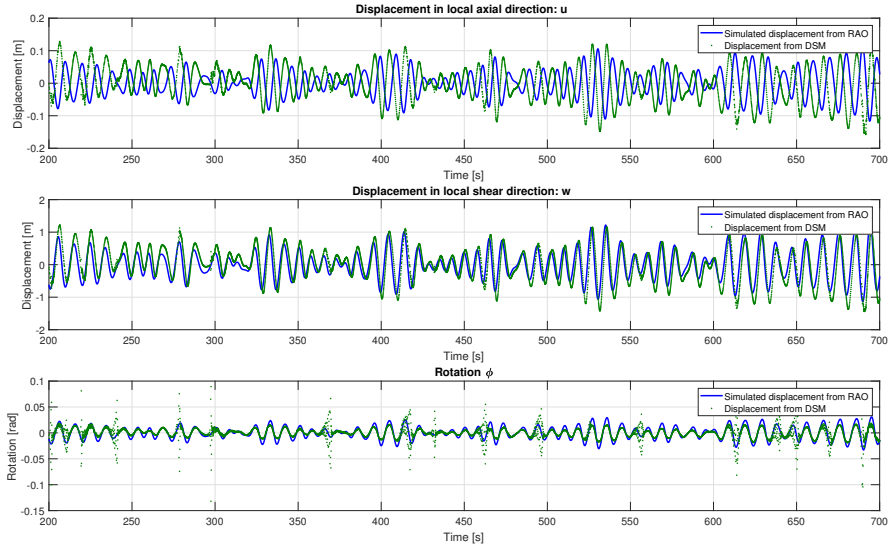

Figure 5.19: Response of the lower DSM in Model I: Subroutine without connection forces

The results of the subroutine including the connection forces are shown in figure 5.20. A large phase difference between the global model and the local model is observed. Although the magnitudes are approximately equal. After more investigation, it was discovered that the all the velocities extracted from the Flexcom database are zeros. The damping and the phase shift are therefore not included in the calculations, since these depend on the velocity.

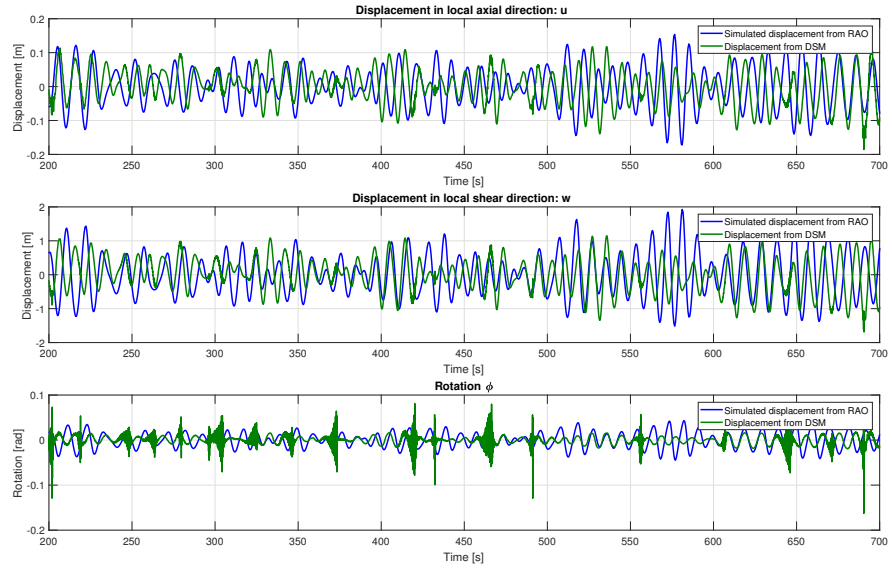

Figure 5.20: Response of the lower DSM in Model I: Subroutine including connection forces

Model II: Seabed to upper DSM

The second model that was used to verify the DSMs is a pipeline from the seabed to the upper DSM, see figure 5.21. Again this model was analysed with two different subroutines, the same as is explained in the previous section.

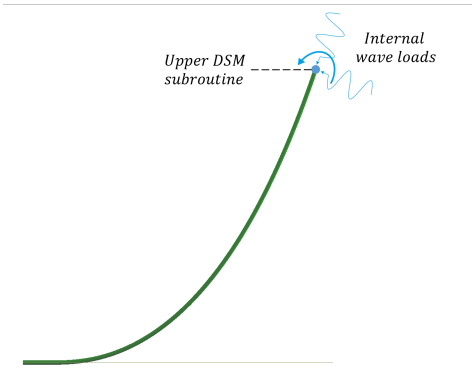

Figure 5.21: Overview of model II in Flexcom

Results of Model II

The responses of this model, using the subroutine without connection forces, do not approximate the global response at all. Furthermore, a second harmonic occurs, thus the damping effect of the DSM is not working correctly. This model configuration needs to be investigated and improved.

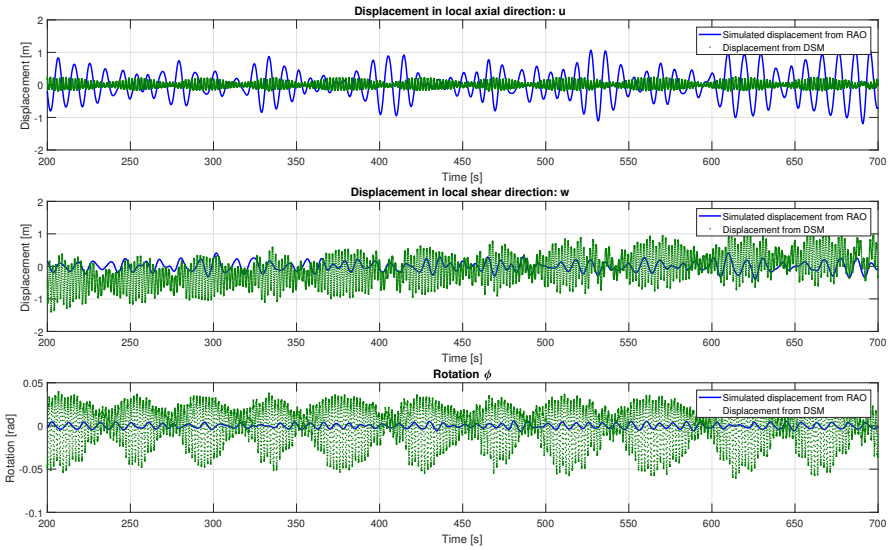

Figure 5.22: Response of the upper DSM in Model II

The model that uses the subroutine with the connection forces did not converge. Several approaches with different ramps, time steps and tolerances were used but unfortunately none of them resulted in graphs that can be shown. Again more research into this subroutine is needed.

Model III: Sagbend with both DSMs

The third and final model is the sagbend with both end constrained by the DSM subroutines, see figure 5.23.

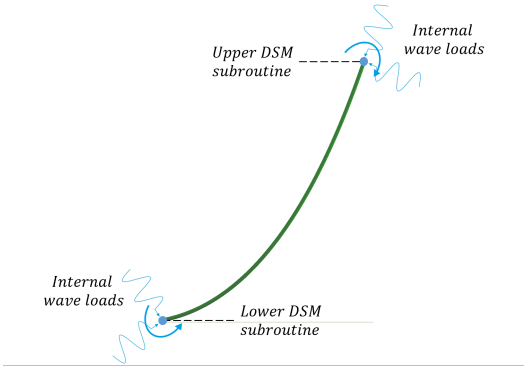

Figure 5.23: Overview of model III: the sagbend model in Flexcom

This model only used the subroutines without the connections forces. Since the subroutine with connection forces did not function for the model of the the upper DSM, the model with these subroutines is disregarded. The assessment of this sagbend model is the ultimate goal of the demonstration and this thesis. The results of this assessment are shown in section 5.3.3.

5.3.2. DSM

The DSMs at the cut-offs of the sagbend are needed for the demonstration of the methodology. These DSMs need to be calculated at the same frequency as the period used for the wave spectrum calculations, so the DSMs at $T = 10$ s are used. The DSMs were calculated at the maximum simulated load, shown in the graphs in section 5.2. If there was no response at the value of the maximum simulated load, the linear response from higher loads was extrapolated and calculated at these values. This results in the the following DSM for the top part, see equation 5.15.

$$\mathbf{DSM_{upper}} = \begin{bmatrix} 1.71\cdot10^{6}+5.26\cdot10^{6}i & 2.17\cdot10^{5}+3.02\cdot10^{5}i & 2.04\cdot10^{6}+2.50\cdot10^{6}i \\ 2.78\cdot10^{5}+2.12\cdot10^{5}i & 2.08\cdot10^{3}+1.35\cdot10^{4}i & 1.18\cdot10^{4}+1.14\cdot10^{5}i \\ 2.47\cdot10^{6}+2.02\cdot10^{6}i & 1.20\cdot10^{4}+1.25\cdot10^{5}i & 6.16\cdot10^{6}+1.05\cdot10^{6}i \end{bmatrix} \tag{5.15}$$

And the lower DSM, see equation 5.16:

$$\mathbf{DSM_{lower}} = \begin{bmatrix} 1.01\cdot10^{7}-1.97\cdot10^{4}i & -1.08\cdot10^{6}+2.02\cdot10^{4}i & 8.11\cdot10^{6}-1.55\cdot10^{5}i \\ -1.07\cdot10^{6}+3.27\cdot10^{4}i & 1.24\cdot10^{5}-3.98\cdot10^{3}i & -1.03\cdot10^{6}+3.16\cdot10^{4}i \\ 7.80\cdot10^{6}-2.28\cdot10^{5}i & -1.01\cdot10^{6}+2.72\cdot10^{4}i & 1.28\cdot10^{7}+2.24\cdot10^{5}i \end{bmatrix} \tag{5.16}$$

The DSMs are inserted into the Flexcom FEM model with the use of a subroutine. In this subroutine the displacements from the Flexcom analysis are extracted and multiplied with the DSM, resulting in the reaction forces at the location of the DSM. Since the analysis is in the time domain, the DSMs, that are in the frequency domain, need to be de-constructed into a mass matrix **M**, a stiffness matrix **K** and a damping matrix **C**. Taking an entry of the DSM that is in the form $a_{m,n} + ib_{m,n}$ we can separate the real part, which is the stiffness, and the imaginary part, which is the damping. The relation to **M**, **K** and **C** is as following:

$$\text{On the diagonal:} a_{m,n} > 0 \Rightarrow K_{m,n} = a_{m,n} \tag{5.17}$$

$$\text{On the diagonal:} a_{m,n} < 0 \Rightarrow M_{m,n} = \frac{-a_{m,n}}{\omega^2} \tag{5.18}$$

$$C_{m,n} = \frac{b_{m,n}}{\omega} \tag{5.19}$$

Where m and n are the indices of the matrix entry and ω is the frequency. When $a < 0$ on the diagonal of the

matrix the system is inertia dominated and therefore the mass matrix is used.
Note that the values of the DSMs changed after this revision, but these DSMs were the ones that were used for the subroutine analyses.

5.3.3. Results of the demonstration

The response of the lower DSM approaches the global response. There is however a second harmonic present and a phase shift has occurred. The imaginary part of the DSM needs to be improved.

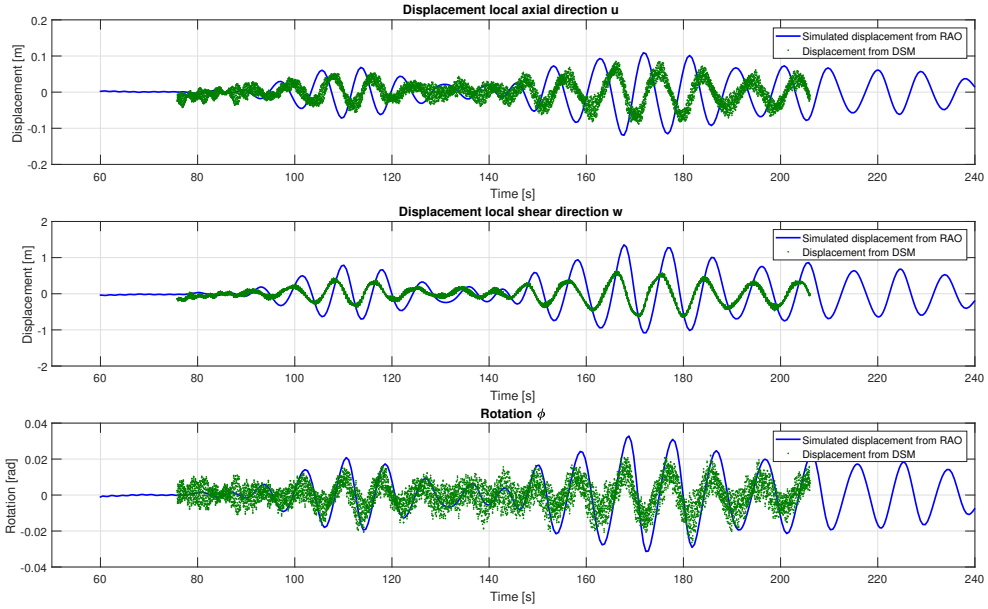

Figure 5.24: Response of the lower DSM in Model III

The response of the upper DSM is completely incorrect. This is very peculiar, since the lower DSM gives a promising response and is directly connected to the upper DSM. Such a large difference in response was not expected.

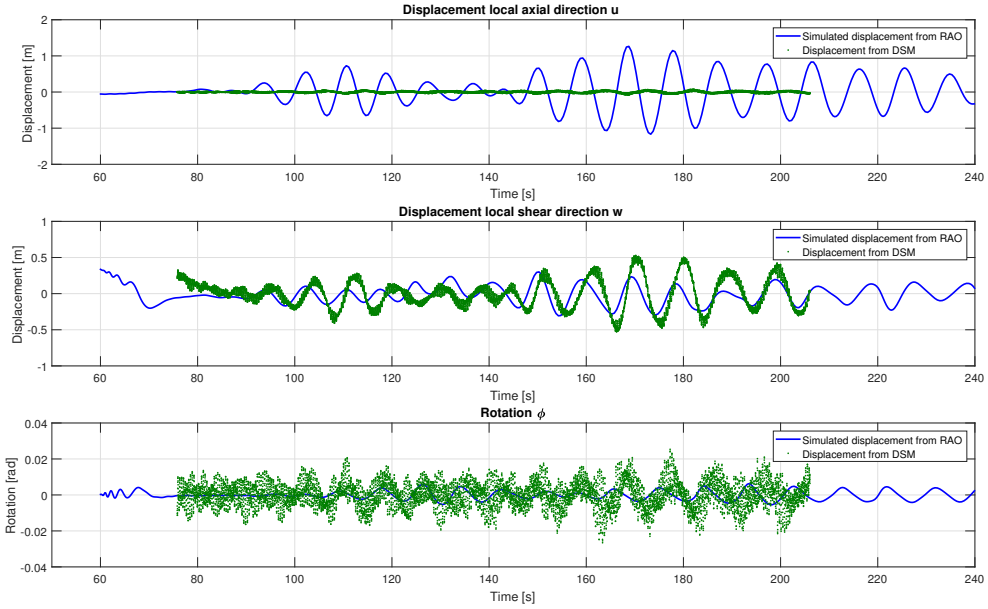

Figure 5.25: Response of the upper DSM in Model III

5.4. Conclusion of the FEM demonstration

Although the results of the bottom part look promising, more research is needed to improve the dynamic FEM assessment of a pipeline with the use of dynamic substructuring. Currently too many errors occur and the simulations take too much computational time. Therefore, more research is needed on the subroutines in a FEM software package and the application of these subroutines on a local pipeline model. It is important to state that the graphs from the FEM analyses should not be used as the basis for future research, the use of the analytical model as a base case would be a better starting point for future research.

6 Discussion

This research has led to a better understanding of behaviour of the sagbend under harmonic excitation and the possibilities of analysing the dynamic behaviour of the sagbend with the use of Frequency Based Substructuring. In this chapter the validity of the research will be discussed, along with its limitations.

6.1. Flexcom software

- The non-linear coupling between displacement DOFs in Flexcom influenced the dynamic stiffness matrices. It is difficult to determine whether the response was influenced by the non-linear coupling or by the actual behaviour.
- The noisy responses at low amplitude complicated the calculations of the DSMs and linear domain analysis.

6.2. Demonstration with Flexcom software

- The proposed demonstration with the use of the Abaqus software was not achieved due to time constraints.
- The demonstration with Flexcom and the subroutines was very time consuming due to database connection. With each iteration a database was opened to be read, closed, opened to write and closed again. This made the runs extremely time consuming.
- The subroutine simulations for the top part did not converge due to high loads at the start up. A long ramp time was needed to eliminate these start up problems.

7

Conclusion and recommendations

7.1. Conclusion

In this section the conclusions with respect to the research question: *How could Frequency Based Dynamic Substructuring improve and speed up the dynamic FEM assessment of a pipe section in the sagbend region, without affecting robustness and reliability?*, are drawn. The conclusions are divided into the subcategories Analytical Demonstration, Linear response analysis and the Flexcom demonstration.

7.1.1. Analytical demonstration

It was necessary to demonstrate the enhanced methodology on an analytical model to prove that the enhanced methodology works and is an efficient method of assessing local models. The following can be concluded from the analytical demonstration:

- Dynamic substructuring method gives correct results for analytical models, different properties were used and all resulted in identical responses for the global and local model. One scenario is shown in figure 4.10.
- It is a simplified representation of the system but nevertheless the results show that the dynamic substructuring method is applicable to these kinds of problems and is promising for the improvement of FEM assessments of pipelines.

7.1.2. Linear response analysis

In order to use the dynamic substructuring method, the regarded system needs to be (approximately) linear. Therefore, the linearity of the system has been studied in section 5.2. The conclusions from this analysis are summarized in the list below:

- For this pipeline configuration each DOF has a amplitude range for which the response is linear and thus the dynamic stiffness methodology is applicable. The downside to this, is that it is time consuming to determine these linear ranges.
- The critical sea state scenario of this configuration is within the linear domain of almost all of the DOFs. The only exceptions are the shear force and the moment of the top part, but these loads are small and thus negligible for the top part.
- It is possible to calculate DSMs with the Flexcom software.
- For the bottom part the responses for the excitation with $T = 10$ s are larger than with $T = 20$ s. For the top part this is vice versa. This is due to the natural period of these parts and their specific configuration. The natural period of the bottom part is $T \approx 6$ s and for the top part $T \approx 23$ s.
- For this configuration the rotational responses are not influenced by the different excitation periods.

7.1.3. Demonstration with Flexcom software

The final section of conclusions to answer the research question, is that regarding the demonstration using the Flexcom software.

- Model I with the lower DSM connected to the vessel shows promising results without the connection forces, see figure 5.19, but still some errors occur. The cause of these errors, model or numerical, needs to be investigated.
- Model II, consisting of the upper DSM connected to the seabed, does not result in good responses, see figure 5.22. This is mainly due to the problems at the start up of the assessment and issues with the implementation of the damping. Note that from the new method of calculating the DSMs some errors in the DSMs occur, this could explain the failed assessment of the top part.
- The velocity cannot be extracted from the Flexcom database. The damping and phase shift are therefore not correctly implemented into the subroutine.
- The final model, Model III, is the model with the sagbend region and the DSMs at both ends. Again the lower DSM responses approach the global response, but a second harmonic is present, see figure 5.24. The upper DSM however gives erroneous responses and also has a second harmonic, see figure 5.25. The damping issues could improve the responses, but the large difference in the accuracy of the responses of the two points connected via a pipeline is very odd. Since the pipeline acts as stiff coupling between the two points, the response should be relatively similar, i.e. both wrong or both correct.

The final conclusion is that the dynamic substructuring is a quick and effective method for analysing dynamic models. Although the application of the method to FEM was not successful, the application to the analytical model proved that it is still a promising method. Further research should be performed on the use of dynamic stiffness matrices in a subroutine. The graphs from the FEM demonstration should however not be used as a reference in future research, since they are not reliable.

7.2. Recommendations for future research

This research has studied the possibility to improve the FEM assessment of pipelines with dynamic sub-structuring. This is proven for an analytical equivalent model, but not for the actual FEM assessment. Several recommendations to improve the dynamic stiffness matrices and the application of these on a local FEM model are suggested and shown in the list below:

- Make the orientation of the static reaction forces time dependent, i.e. with same orientation with respect to the pipe instead of fixed in the global axis system, possibly with a subroutine. For small perturbations it is not problematic, but it is more accurate if this done.
- Make the orientation of the excitation force time dependent so that it is always in the correct orientation with respect to the pipe segment, possibly with a subroutine. Again for small perturbations it is not problematic, but it is more accurate if the excitation follows the orientation of the pipe segment.
- Apply the linear analysis to other pipeline configurations to increase the database.
- Improve the soil interaction of the pipeline model. This results in a more realistic response of the bottom part of the model.
- Perform a more elaborate validation of the enhanced method. More runs with both the Flexcom and Abaqus software.
- Make the DSMs frequency dependent in order to make the application more robust.
- Compare the model set-up of the analytical model to the Flexcom models to locate potential differences or mistakes.
- Build the analytical model in the Flexcom software. The calculation of the DSMs can be verified and the results of this Flexcom analysis can be compared to the results of the analytical model.

Bibliography

[1] D De Klerk, D J Rixen, and S N Voormeeren. General Framework for Dynamic Substructuring: History, Review, and Classification of Techniques. doi: 10.2514/1.33274.

[2] Dennis de Klerk, Daniel J. Rixen, and Jasper de Jong. *The Frequency Based Substructuring (FBS) Method reformulated according to the Dual Domain Decomposition Method.* 2006.

[3] Det Norske Veritas. *Offshore Standard: Submarine Pipeline Systems DNV-OS-F101.* 2013.

[4] J. M. J. Journée and W. W. Massie. *Offshore Hydromechanics.* 2001.

[5] Krishna Chaitanya Konjerla. *FRF Based Experimental – Analytical Dynamic Substructuring Using Transmission Simulator.* 2016.

[6] Daryl L. Logan. *A first course in the finite element method.* 2011. ISBN 978-0495668251.

[7] Richard Ogink. *Dynamics of a deepwater suspended pipeline during J-lay.* 2003.

[8] B Mutlu Sumer and Jørgen Fredsøe. *Hydrodynamics Around Cylindrical Structures, Revised Edition.* 2006. ISBN 978-981-270-039-1.

[9] Paul Van Der Valk. *Coupled Simulations of Wind Turbines and Offshore Support Structures.* PhD thesis, 2014.

[10] Wood Group Kenny Ireland. *Technical Manual Flexcom.* 2014.

A

Amplitude ranges

Table A.1: Force amplitude range top part

Top Part	Axial			Shear			Moment		
Percentage	**Amplitude**	**Total Force**	**Unit**	**Amplitude**	**Total Force**	**Unit**	**Amplitude**	**Moment**	**Unit**
0%	0.00	586.25	kN	0.00	170.06	N	0.00	43.07	kNm
1%	5.86	592.11	kN	1.70	171.76	N	0.43	43.50	kNm
5%	29.31	615.56	kN	8.50	178.56	N	2.15	45.22	kNm
10%	58.63	644.88	kN	17.01	187.07	N	4.31	47.38	kNm
15%	87.94	674.19	kN	25.51	195.57	N	6.46	49.53	kNm
20%	117.25	703.50	kN	34.01	204.07	N	8.61	51.68	kNm
30%	175.88	762.13	kN	51.02	221.08	N	12.92	55.99	kNm
40%	234.50	820.75	kN	68.02	238.08	N	17.23	60.30	kNm
50%	293.13	879.38	kN	85.03	255.09	N	21.54	64.61	kNm
60%	351.75	938.00	kN	102.04	272.10	N	25.84	68.91	kNm
70%	410.38	996.63	kN	119.04	289.10	N	30.15	73.22	kNm
80%	469.00	1055.25	kN	136.05	306.11	N	34.46	77.53	kNm
90%	527.63	1113.88	kN	153.05	323.11	N	38.76	81.83	kNm
100%	586.25	1172.50	kN	170.06	340.12	N	43.07	86.14	kNm
125%	732.81	1319.06	kN	212.58	382.64	N	53.84	96.91	kNm
150%	879.38	1465.63	kN	255.09	425.15	N	64.61	107.68	kNm
180%	1055.25	1641.50	kN	306.11	476.17	N	77.53	120.60	kNm
200%	1172.50	1758.75	kN	340.12	510.18	N	86.14	129.21	kNm
250%	1465.63	2051.88	kN	425.15	595.21	N	107.68	150.75	kNm
400%	2345.00	2931.25	kN	680.24	850.30	N	172.28	215.35	kNm
500%	2931.25	3517.50	kN	850.30	1020.36	N	215.35	258.42	kNm
750%	4396.88	4983.13	kN	1275.45	1445.51	N	323.03	366.10	kNm
1000%	5862.50	6448.75	kN	1700.60	1870.66	N	430.70	473.77	kNm
1500%	8793.75	9380.00	kN	2550.90	2720.96	N	646.05	689.12	kNm
2000%	11725.00	12311.25	kN	3401.20	3571.26	N	861.40	904.47	kNm
3000%	17587.50	18173.75	kN	5101.80	5271.86	N	1292.10	1335.17	kNm

Table A.2: Force amplitude range bottom part

Bottom part	**Axial**			**Shear**			**Moment**		
Percentage	**Amplitude**	**Total Force**	**Unit**	**Amplitude**	**Force**	**Unit**	**Amplitude**	**Moment**	**Unit**
0%	0.00	190.95	kN	0.00	1.36	kN	0.00	360.49	kNm
1%	1.91	192.86	kN	0.01	1.37	kN	3.60	364.09	kNm
5%	9.55	200.50	kN	0.07	1.43	kN	18.02	378.51	kNm
10%	19.10	210.05	kN	0.14	1.50	kN	36.05	396.54	kNm
15%	28.64	219.59	kN	0.20	1.56	kN	54.07	414.56	kNm
20%	38.19	229.14	kN	0.27	1.63	kN	72.10	432.59	kNm
30%	57.29	248.24	kN	0.41	1.77	kN	108.15	468.64	kNm
40%	76.38	267.33	kN	0.54	1.90	kN	144.20	504.69	kNm
50%	95.48	286.43	kN	0.68	2.04	kN	180.25	540.74	kNm
60%	114.57	305.52	kN	0.82	2.18	kN	216.29	576.78	kNm
70%	133.67	324.62	kN	0.95	2.31	kN	252.34	612.83	kNm
80%	152.76	343.71	kN	1.09	2.45	kN	288.39	648.88	kNm
90%	171.86	362.81	kN	1.22	2.58	kN	324.44	684.93	kNm
100%	190.95	381.90	kN	1.36	2.72	kN	360.49	720.98	kNm
125%	238.69	429.64	kN	1.70	3.06	kN	450.61	811.10	kNm
150%	286.43	477.38	kN	2.04	3.40	kN	540.74	901.23	kNm
180%	343.71	534.66	kN	2.45	3.81	kN	648.88	1009.37	kNm
200%	381.90	572.85	kN	2.72	4.08	kN	720.98	1081.47	kNm
250%	477.38	668.33	kN	3.40	4.76	kN	901.23	1261.72	kNm
400%	763.80	954.75	kN	5.44	6.80	kN	1441.96	1802.45	kNm
500%	954.75	1145.70	kN	6.80	8.16	kN	1802.45	2162.94	kNm
750%	1432.13	1623.08	kN	10.20	11.56	kN	2703.68	3064.17	kNm
1000%	1909.50	2100.45	kN	13.60	14.96	kN	3604.90	3965.39	kNm
1500%	2864.25	3055.20	kN	20.40	21.76	kN	5407.35	5767.84	kNm
2000%	3819.00	4009.95	kN	27.20	28.56	kN	7209.80	7570.29	kNm
3000%	5728.50	5919.45	kN	40.80	42.16	kN	10814.70	11175.19	kNm

B

Connection forces

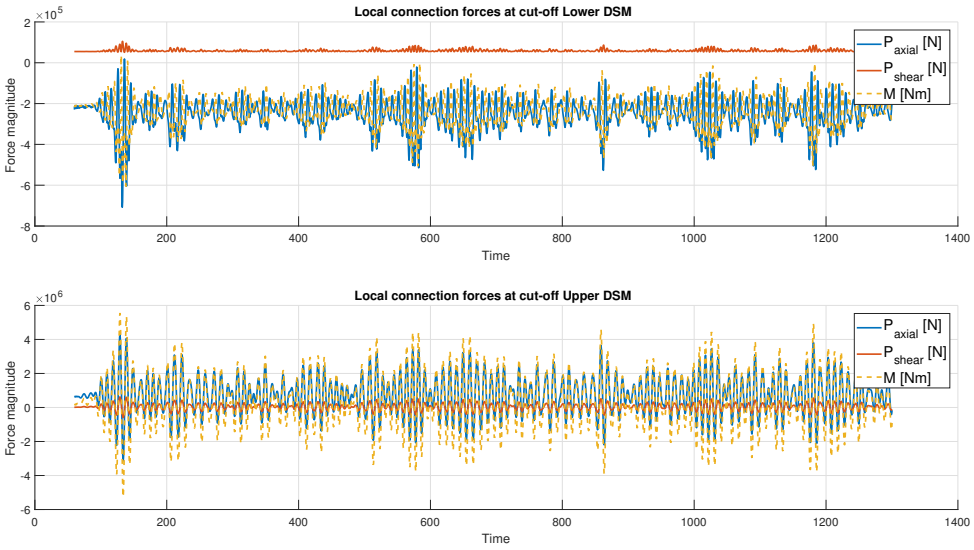

Figure B.1: Local connection forces at the DSMs

List of Figures

List of Tables